이학박사 학위논문

The Role of Mll4 in Myofiber Maintaining Muscle Stem Cells

근육줄기세포군 유지를 위한

근섬유 내 Mll4의 역할 연구

2025년 2월

서울대학교 대학원

생명과학부 생명과학전공

김 예 은

근육줄기세포군 유지를 위한
근섬유 내 M114의 역할 연구

지도 교수 공 영 윤

이 논문을 이학박사 학위논문으로 제출함

2025년 2월

서울대학교 대학원

생명과학부 생명과학전공

김 예 은

김예은의 이학박사 학위논문을 인준함

2025년 2월

위 원 장 이 건 수 (인)

부위원장 공 영 윤 (인)

위 원 김 진 홍 (인)

위 원 신 근 유 (인)

위 원 김 지 훈 (인)

The Role of Mll4 in Myofiber Maintaining Muscle Stem Cells

Young-Yun Kong

Submitting a Ph.D. Dissertation of

Biological Sciences

February 2025

Graduate School of Biological Sciences

Seoul National University

Biological Science Major

Yea-Eun Kim

Confirming the Ph.D. Dissertation written by

Yea-Eun Kim

February 2025

Chair	Kunsoo Rhee (Seal)
Vice Chair	Young-Yun Kong (Seal)
Examiner	Jin-Hong Kim (Seal)
Examiner	Kunyoo Shin (Seal)
Examiner	Ji-Hoon Kim (Seal)

Abstract

The Role of Mll4 in Myofiber Maintaining Muscle Stem Cells

Yea Eun, Kim

School of Biological Sciences

The Graduate School

Seoul National University

Muscle stem cells (MuSCs) undergo numerous state transitions throughout life, which are critical for supporting normal muscle growth and regeneration. Therefore, it is crucial to investigate the regulatory mechanisms governing the transition of MuSC states across different postnatal developmental stages. Here, I observed that *Mll4* is crucial for maintaining MuSCs in both pubertal and adult muscles, which may be accomplished through the modulation of distinct Notch ligand expressions in myofibers. Myofiber-specific *Mll4*-deleted mice during postnatal myogenesis were observed with increased number of cycling MuSCs that proceeded to a differentiation state, leading to MuSC deprivation. When *Mll4* was ablated in adult

muscles using the inducible method, adult MuSCs lost their quiescence and differentiated into myoblasts, also causing the depletion of MuSCs. Such roles of *Mll4* in myofibers coincided with decreased expression levels of distinct Notch ligands: *Jag1* and *Dll1* in juvenile and *Jag2* and *Dll4* in adult muscles, indicating a unique function of *Mll4* in myofibers controlling MuSC state, possibly by orchestrating different Notch ligand expression in various developmental stages. Together, my study suggests that *Mll4* in myofibers regulates MuSCs by potentially modulating Notch signaling in both pubertal and adult muscles.

Keywords: Skeletal muscle, muscle stem cell, myogenesis, muscle injury, Myeloid/lymphoid or mixed-lineage leukemia 4 (Mll4), Notch signaling

Student number: 2020-25562

Table of Contents

List of Figures

List of Tables

General Information

Skeletal Muscle

Skeletal muscle is a tissue that enables mammals to move voluntarily, maintain posture, and process various metabolic pathways (Frontera and Ochala, 2015). Neural signals are conducted to skeletal muscles via the neuromuscular junction where acetylcholine is secreted at the end of motor neurons, triggering the release of calcium ions from the sarcoplasmic reticulum that initiates muscle contraction (Witzemann, 2006). The contraction of muscles leads to the movement of bones, as muscles are attached to them via tendons, generating mechanical forces to drive voluntary movements. The contractile units of the muscles, sarcomeres, are composed of the arrangement of actin and myosin filaments, which appear as a striated pattern in skeletal muscles (Frontera and Ochala, 2015). Long, multinucleated cells called muscle fibers are the basic cellular component of skeletal muscles, which are bundled into fascicles. Connective tissues such as the epimysium, perimysium, and endomysium surround the fascicle, providing structural integrity and support (Frontera and Ochala, 2015). In addition to movement, skeletal muscles play a crucial role in controlling metabolism by consuming energy-high substances such as glucose and fatty acids, generating heat during contraction, and secreting hormone-like molecules that can have a whole-body impact (Frontera and Ochala, 2015)

Figure 1. Skeletal muscle anatomy and structure. Skeletal muscle is connected to bones via tendons to provide voluntary movements. Myofibers, which are cylindrical, multinucleated cells, are enclosed by a connective tissue called the endomysium and grouped into bundles known as fascicles, which are surrounded by the perimysium. These fascicles are further wrapped in an outer connective tissue layer called the epimysium. Myonuclei and muscle stem cells are located along the surface of the myofibers.

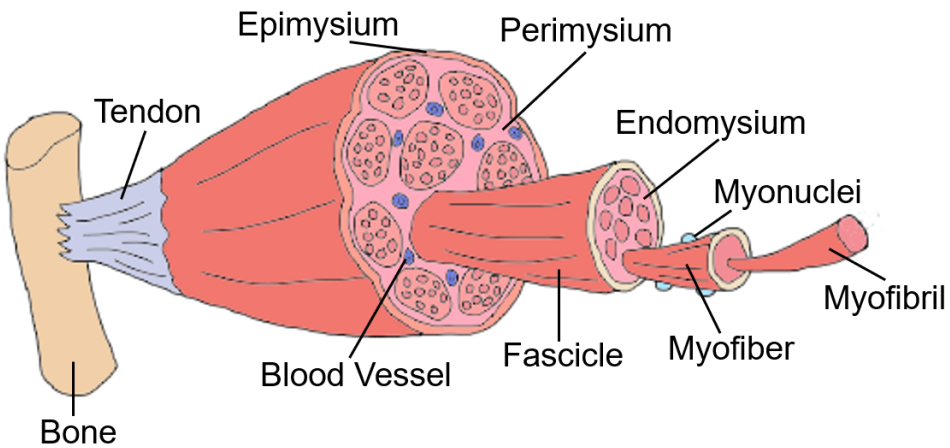
Epimysium
Perimysium
Tendon
Endomysium
Myonuclei
Myofibril
Blood Vessel
Fascicle
Myofiber
Bone

Myogenesis

Myogenesis is a biological term that indicates the formation of skeletal muscle tissue that occurs during both embryonic/fetal development and postnatal muscle regeneration during adulthood (Kang and Krauss, 2010; Tajbakhsh, 2009). In the early stage of embryogenesis, myogenic transcription factors that belong to the myogenic regulatory factor (MRF) family such as MyoD and Myf5 are expressed in mesodermal progenitor cells (Hernandez-Hernandez et al., 2017). This leads to cellular differentiation into myoblasts that proliferate and fuse into myotubes, which later become mature myofibers. This process persists until puberty when myoblast proliferation halts and starts to form a quiescent muscle stem cell pool (Kim et al., 2016). These adult muscle stem cells, also known as satellite cells reside under the basal lamina of muscle fibers (Hernandez-Hernandez et al., 2017).

Upon injury in adult muscle tissues, quiescent muscle stem cells are activated and migrate outside of the basal lamina. They enter the cell cycle, differentiate into myogenic committed cells, and fuse into damaged myofibers to repair and generate new myofibers. This process recapitulates the aspects of developmental myogenesis (Best et al., 2000). Dynamic molecular signaling pathways such as Notch and Wnt4 as well as growth factors are involved in the process (Kim et al., 2016; Eliazer et al., 2022; Eliazer et al., 2019). Moreover, cellular components like immune cells and fibro-adipogenic progenitors (FAPs) contribute to providing the optimal environment for tissue repair (Farup et al., 2015).

Figure 2. Progressive phases of myogenesis. During embryonic myogenesis, myogenic cells proliferate and fuse to form primary myotubes. Fetal myogenesis occurs when secondary myotubes form around the primary myotubes. These myotubes differentiated into mature myofibers. After birth, myofibers continue to grow through the proliferation and differentiation of MuSCs. During puberty, when sex hormone is released, MuSCs enter quiescence.

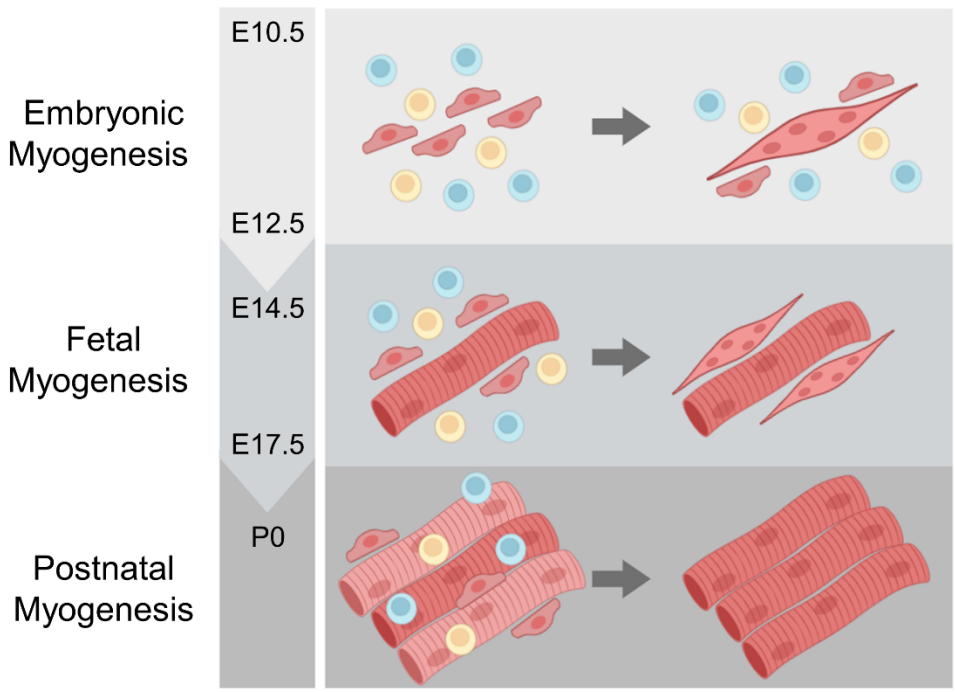
Embryonic Myogenesis
E10.5
E12.5
Fetal Myogenesis
E14.5
E17.5
Postnatal Myogenesis
P0

Myofiber type and exercise capacity

Skeletal muscle fibers are grouped into slow-twitch (type I) and fast-twitch (type II) fibers, which are adapted to different functions and demands (Egan and Zierath, 2013). Slow-twitch fibers are also known as 'red fibers' due to their rich containment of myoglobin, mitochondria, and blood vessels. They primarily rely on oxidative metabolism, which enables efficient energy production. This facilitates fatigue resistance, which empowers slow-twitch fibers to tolerate prolonged movement like endurance exercise. In contrast, fast-twitch fibers rely on anaerobic metabolism to generate rapid and powerful contractions. fast-twitch fibers are divided into subtypes - type IIa (oxidative-glycolytic) and type IIb/x (glycolytic) - depending on their reliance on anaerobic (glycolytic) metabolism. The glycolytic metabolism enables fast-twitch fibers to generate power to execute high-intensity exercise such as weightlifting, but not endurance exercise because the metabolic process produces byproducts that accumulate in muscles (Schiaffino and Reggiani, 2011). Genetics predispose the proportion of slow- and fast-twitch fibers in muscles, but muscle adaptation after physical activity or environmental stress can alter myofiber composition.

Figure 3. Muscle fiber type and their characteristics. Muscle fibers are categorized into three main types based on their metabolic and contractile properties: type I (slow-twitch), type IIa (fast-twitch oxidative) and type IIx (fast-twitch glycolytic).

Characteristics	**Type 1**	**Type 2A**	**Type 2B/X**
Contraction Time	Slow	Fast	Very Fast
Oxidative Capacity	High	High	Low
Diameter	Small	Medium	Large
Resistance to Fatigue	High	Moderate	Small
Generating Force	Small	Moderate	Very High
Myoglobin	High	Medium	Low
Mitochondria	Many	Moderate	Few

Muscle stem cells

Muscle stem cells (MuSCs), also known as satellite cells, are fundamental for the development, growth, maintenance, and regeneration of skeletal muscle tissue. During embryonic development, the paraxial mesoderm is segmented into somites (Burke and Nowicki, 2003; Nassari et al., 2017). Progenitor cells in the somites are guided to commitment to the myogenic lineage when molecular signals such as Pax3 and Pax7 are activated (Hernandez-Hernandez et al., 2017). Committed myoblasts actively proliferate to contribute to the development and growth of muscle tissue until the juvenile stage. During puberty, sex hormones induce activated MuSCs to exit the cell cycle and enter a dormant, quiescent state. This enables muscle to store a reserve stem cell pool (Kim et al., 2016). Quiescent adult MuSCs are re-activated by injury or stress. MuSCs enter the cell cycle to proliferate and differentiate into myogenic cells that express MyoD and myogenin (Hernandez-Hernandez et al., 2017). Differentiated myoblasts fuse into existing myofibers to repair damaged muscle tissue or fuse with one another to generate new myofibers (Tajbakhsh, 2009). When the regeneration process is done, MuSCs re-enter quiescence to maintain the stem cell pool. The dynamic and balanced transition of the MuSCs state ensures efficient muscle adaptation and repair throughout the lifespan.

Figure 4. Dynamic state transition of MuSCs throughout developmental stages. MuSCs actively proliferate and differentiate into myocytes during juvenile stages. During puberty, cycling MuSCs exit the cell cycle and enter a quiescent state to form a reserve MuSC pool in adult muscles. Stress such as injury causes quiescent MuSCs to re-enter the cell cycle and differentiate into myocytes to repair damaged tissues. After regeneration, MuSCs return to quiescence.

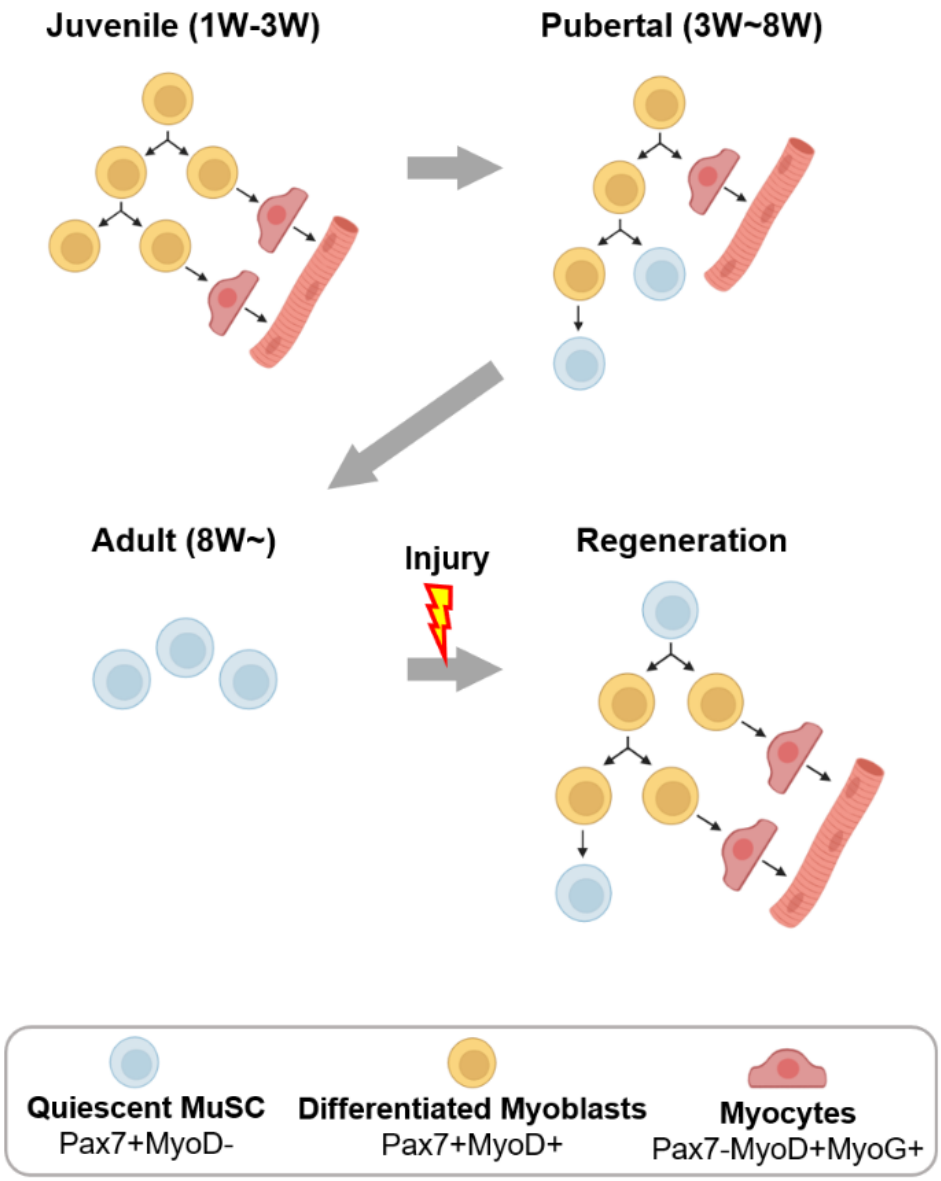
Juvenile (1W-3W)
Pubertal (3W~8W)
Adult (8W~)
Injury
Regeneration
Quiescent MuSC
Pax7+MyoD-
Differentiated Myoblasts
Pax7+MyoD+
Myocytes
Pax7-MyoD+MyoG+

Mixed-lineage leukemia 4

Mixed-lineage leukemia 4 (Mll4), also known as KMT2D, is a histone mono- or di-methyltransferase that is first identified as part of the MLL family (Lee et al., 2013; Wang et al., 2016). It plays an essential role as an epigenetic regulator by remodeling chromatin. Mll4 catalyzes the methylation of histone H3 at lysine 4 (H3K4me1), which is a key epigenetic modulation associated with enhancer activation, thereby influencing gene expression during tissue differentiation and maintenance (Wang et al., 2017; Lai et al., 2017). Recent studies on Mll4 uncovered its involvement in various biological processes, including stem cell maintenance, tumorigenesis, and adipogenesis (Wang et al., 2017; Dhar et al., 2018; Lai et al., 2017). Particularly, mutations in the human MLL4 gene have been associated with Kabuki syndrome, where affected individuals are observed with developmental delay and intellectual disability (Malvin et al., 2022). Considering the multifunctional role of Mll4, it is important to make a focal point for understanding its specific contributions to skeletal muscle, as these may have significant implications for tissue health.

Figure 5. Histone methylation by the Mll4 complex. Mll4 recruits various pioneer transcription factors to detect and attach to the direct anchoring site. By marking H3K4-methylation in enhancer regions, Mll4 activates gene transcription. When chromatin remodelers such as the BAF (SWI/SNF) complex are recruited, enhancer-promoter loops are formed, enabling the activation of indirect target sites.

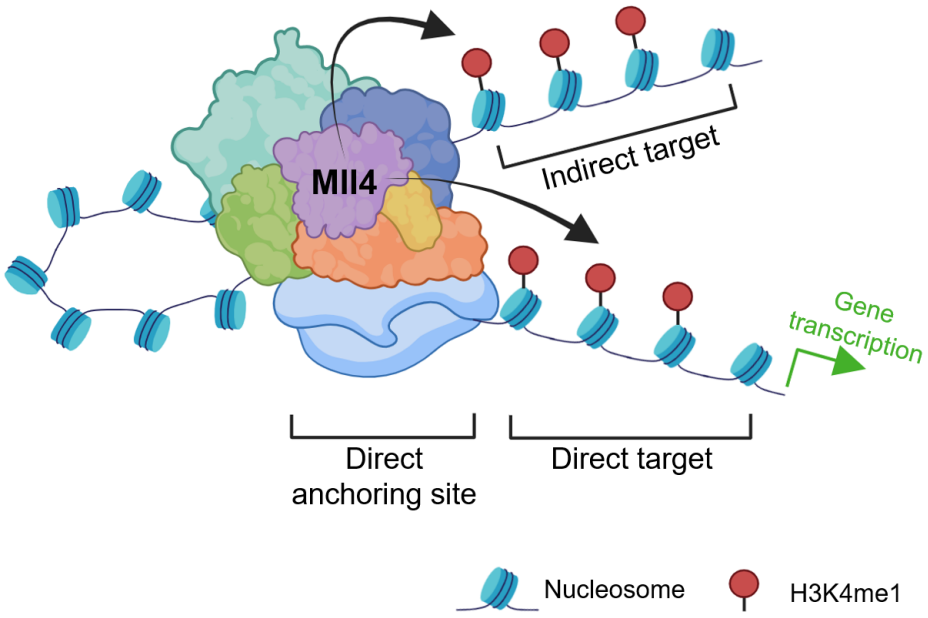
MII4
Indirect target
Gene transcription
Direct anchoring site
Direct target
Nucleosome
H3K4me1

Notch signaling pathway

The Notch signaling pathway is highly conserved intracellular signaling that determines cell fate decision, proliferation, and differentiation across various tissues (Siebel et al., 2017; Gioftsidi et al., 2022). Signal-sending cells express Notch ligands, such as Delta-like (DLL) or Jagged. These ligands interact with signal-receiving cells expressing the Notch receptor. The interaction initiates Notch signaling by triggering two sequential proteolytic cleavages by ADAM-family metalloproteases and the γ-secretase complex, which releases the Notch intracellular domain (NICD) from the Notch receptor. The NICD translocates to the nucleus and binds to the transcriptional regulator RBP-Jκ (CBF1 in mammals), recruiting co-activators to activate the expression of Notch target genes such as Hes and Hey family genes (Sprinzak and Blacklow, 2021). Since the Notch signaling pathway relies on direct cell-to-cell contact for initiation and does not require amplification steps, it allows precise spatial and temporal regulation during diverse cellular processes.

In skeletal muscle, the Notch signaling pathway plays a pivotal role in MuSC maintenance and muscle regeneration. During embryonic muscle development, Notch1 and Notch2 collaboratively play a critical role in maintaining proliferating MuSCs (Jo et al., 2022). In pubertal muscles, the Notch ligands Dll1 and Jag1, expressed in myofibers, promote the transition of cycling MuSCs to a quiescent state (Kim et al., 2016). In adult muscles, Dll4 expressed in myofibers sustains the quiescence of adult MuSCs, preventing inappropriate activation (Eliazer et al., 2022). Upon muscle injury, the Notch signaling pathway is dynamically regulated to activate MuSCs, which is subsequently downregulated as MuSCs transit to

differentiation. Disruption of Notch signaling can significantly impair muscle development and regeneration as it is the fundamental signaling pathway for maintaining MuSCs.

Figure 6. Pathway of Notch signaling activation across cells. Notch signaling is initiated through direct cell-cell interactions, where signal-sending cells express Notch ligands (e.g., Delta-like or Jagged) and signal-receiving cells express Notch receptors on the surface. Ligand-receptor binding triggers two sequential cleavages of the receptor, each mediated by ADAM proteases and γ-secretase. This leads to the release of the Notch intracellular domain (NICD), which translocates to the nucleus and associates with transcriptional regulators such as RBPJ to activate target gene expression. Meanwhile, the Notch extracellular domain (NECD), is endocytosed by ubiquitin ligation of Mib1 in the signal-sending cell.

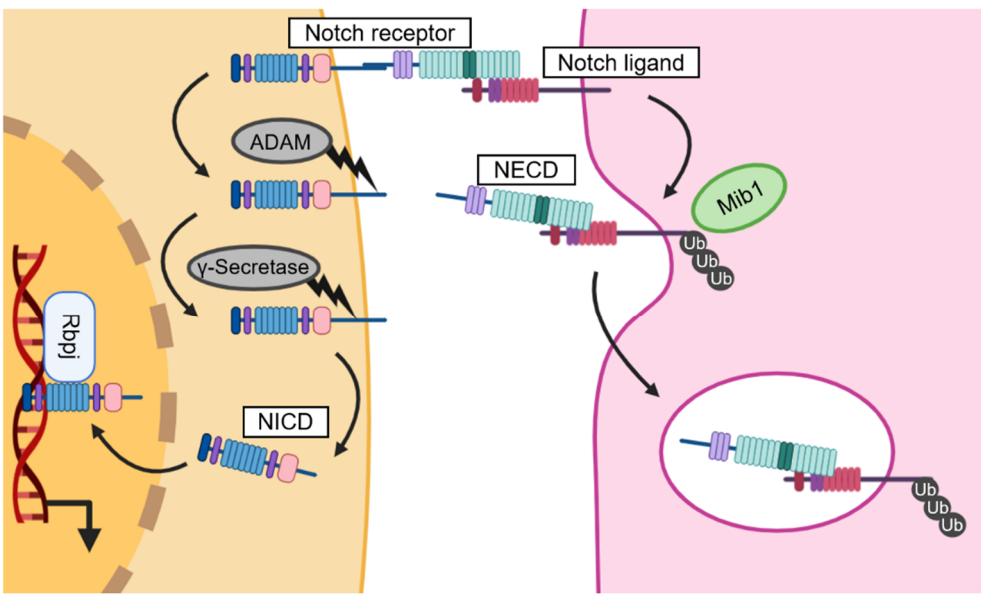
Notch receptor
Notch ligand
ADAM
NECD
Mib1
Ub
Ub
Ub
γ-Secretase
Rbpj
NICD
Ub
Ub
Ub
Signal-receiving Cell
Signal-sending Cell

Introduction

Muscle stem cells (MuSCs) are resident stem cells of skeletal muscle that contribute to muscle development, growth, and regeneration. They actively proliferate and differentiate into myocytes to contribute to myonuclei accretion and muscle growth (White et al., 2010; Kim et al., 2016). In the adult stage, MuSCs enter a quiescent state and remain as reserve stem cells (Mukund et al., 2020; Frontera and Ochala, 2015). Upon injury, MuSCs become activated, providing myogenic cells to repair the muscle tissue. During muscle development and regenerative myogenesis, the MuSC niche regulates the dynamic transitions of MuSCs, including their activation, proliferation, differentiation, and self-renewal.

Myofiber is an important cellular component of the MuSC niche. Unlike other cells that compose the MuSC niche, myofibers are in direct contact with MuSCs (Yin et al., 2013). This enables them to regulate the MuSC state through both paracrine and contact-dependent juxtacrine signaling (Relaix et al., 2021). As paracrine signaling, myofibers secrete Wnt-4 to repress aberrant activation and maintain MuSC quiescence in adult homeostatic muscle (Eliazer et al., 2019). FGF6 is another paracrine factor produced in myofibers to promote MuSC expansion during both developmental and regenerative myogenesis (Zhao et al., 2004; Zofkie et al., 2021). Myofibers also provide juxtacrine signals such as N-cadherin and M-cadherin to maintain MuSCs. These cell adhesion molecules are expressed at myofiber sites that are in direct contact with MuSCs to repress stem cell activation and maintain MuSC

quiescence in adult muscles (Goel et al., 2017).

Among the various molecular signals derived from myofibers, Notch signaling plays a particularly crucial role in the maintenance of the stem cell pool and the regulation of cell fate decisions in MuSCs. In mammals, Notch signal-sending cells express Notch ligands (Dll1, 4 and Jag1, 2) and signal-receiving cells express Notch receptors (Notch1-4) (Siebel and Lendahl, 2017, Gioftsidi et al., 2022). Myofibers activate Notch signaling at different developmental stages primarily to generate a quiescent population of myogenic progenitor cells (Kim et al., 2016, Jo et al., 2022). Several Notch ligands are expressed in myofibers to facilitate diverse Notch signaling to regulate the MuSC niche effectively at different developmental stages. Dll1, a Notch ligand mainly expressed in pubertal myofibers, interacts with the activated MuSCs to promote self-renewal, which is crucial for maintaining MuSCs (Schuster-Gossler et al., 2007; Yartseva et al., 2020; Zhang et al., 2021). In adult myofibers, Dll4 represses MuSC cell cycle entry, thus retaining the quiescent state of MuSCs (Eliazer et al., 2022; Low et al., 2018). While various studies have indicated that Notch signaling originating from myofibers has a role in regulating the state of MuSCs, there is limited understanding of whether there is a regulator present in myofibers that coordinates the expression of Notch ligands among different postnatal periods such as puberty and adulthood.

Mixed-lineage leukemia 4 (MLL4; also known as Kmt2d), a major H3K4 mono- and di-methyltransferase, is an essential histone modification enzyme for

enhancer activation (Lee et al., 2013; Wang et al., 2016; Wang et al., 2017). H3K4me1 marking by MLL4 is required for H3K27 acetylation and the recruitment of cell type-specific transcription factors (Lee et al., 2013; Wang et al., 2016; Wang et al., 2017; Lai et al., 2017). Deletion of *Mll4* results in the disturbance of H3K4me1 and H3K27ac on active enhancers, leading to defects in transcribing both newly activated genes, as well as genes that were already being expressed (Lee et al., 2013; Wang et al., 2016; Wang et al., 2017).

A recent study addressed that *Mll4* depletion in myofibers turns off the slow type I fiber-specific genes, leading to fiber-type transition (Liu et al., 2020). Myofibers are classified into two primary types: Type 1 (slow-twitch) and Type 2 (fast-twitch). Type 1 fibers rely on oxidative metabolism, which endows them with endurance capabilities. In contrast, Type 2 fibers utilize glycolytic pathways to generate rapid force (Schiaffino and Reggiani, 2011). This diversity in myofiber types contributes to muscle performance and adaptability to various stimuli (Pette and Staron, 2000). Liu et al., (2020) reported that endurance exercise capacity was reduced in the Mll4-KO mice due to a slow-to-fast fiber-type shift. However, this study exclusively utilized male mice and focused solely on the function of Mll4 in developing myofibers. Building on these findings, my research aims to further investigate the role of Mll4 in myofibers across both sexes and various developmental stages.

In this paper, I report that MLL4 in myofiber is required to maintain MuSCs

during both the pubertal and adult stages, regardless of gender. Mouse models with myofiber-specific deletion of *Mll4* exhibited reduced myofiber length, fewer myonuclei, and MuSC depletion. When *Mll4* was ablated at the adult stage using an inducible method, MuSCs underwent differentiation into myoblasts, either with or without entering the cell cycle, leading to a depletion of adult MuSCs. Furthermore, the expression of specific Notch ligands at both pubertal and adult stages was significantly reduced in *Mll4*-knockout myofibers. Together, my data suggest the importance of MLL4 in skeletal muscle fibers for maintaining the MuSC number, which might be achieved by affecting Notch ligand expression, in different postnatal periods.

Results

Mll4 deletion in myofiber alters CSA and slow fiber composition in males, but not in female mice

Previously, Liu and colleagues (2020) reported that the deletion of *Mll4* in developing myofibers did not impact overall muscle mass but resulted in changes to muscle characteristics, including an increased cross-sectional area (CSA) and a shift from slow to fast fiber types. However, the results were derived exclusively from male mice. Given that Mll4 is expressed in both sexes (Figure 7A), I investigated whether female mice would exhibit a similar phenotype to males following *Mll4* ablation. I crossed *Mll4*$^{f/f}$ mice that carry loxP sites of the *Mll4* gene (Lee et al., 2013), with *MCK*$^{Cre/+}$ mice (Brü et al., 1998), which produced Mll4$^{\Delta MCK}$ mice (*MCK*$^{Cre/+}$*; Mll4*$^{f/f}$) (Liu et al., 2020). By performing quantitative real-time PCR (qRT-PCR), the deletion of *Mll4* was confirmed in 8-week-old Mll4$^{\Delta MCK}$ myofibers (Figure 7B-C). Muscle weight remained unchanged in 8-week-old Mll4$^{\Delta MCK}$ mice, regardless of sex (Figure 7D-E). As reported (Liu et al., 2020), male Mll4$^{\Delta MCK}$ mice displayed increased CSA (Figure 8A) and fiber type shifts toward a decreased ratio of slow-twitch fiber in soleus muscle (Figure 8B-D). In contrast, no significant differences in these characteristics were observed in Mll4$^{\Delta MCK}$ female mice compared to Mll4^{WT} female mice (Figure 9A-D), suggesting that the alterations in CSA and fiber type composition following the deletion of Mll4 in myofibers may represent a phenotype selectively characteristic of male musculature, potentially attributable to male-specific factors or microenvironments.

Figure 7. Expression level of Mll4 and muscle mass of Mll4^{WT} and Mll4$^{\Delta MCK}$ mice. (A) qRT-PCR analysis to detect Mll4 expression in 8-week-old Mll4^{WT} Male and female. (B, C) qRT-PCR analysis to detect Mll4 exon deletion in myofibers of male (B) and female (C) 8-week-old Mll4$^{\Delta MCK}$ and Mll4^{WT} mice. n=3 mice for each genotype. (D, E) Muscle mass of TA, EDL, GA, and soleus muscle from Mll4^{WT} and Mll4$^{\Delta MCK}$ mice of both males and females. n=3 mice for each genotype. Data are presented as mean ± SEM of biological replicates. Statistical analyses were performed using unpaired t-test with Welch's correction.

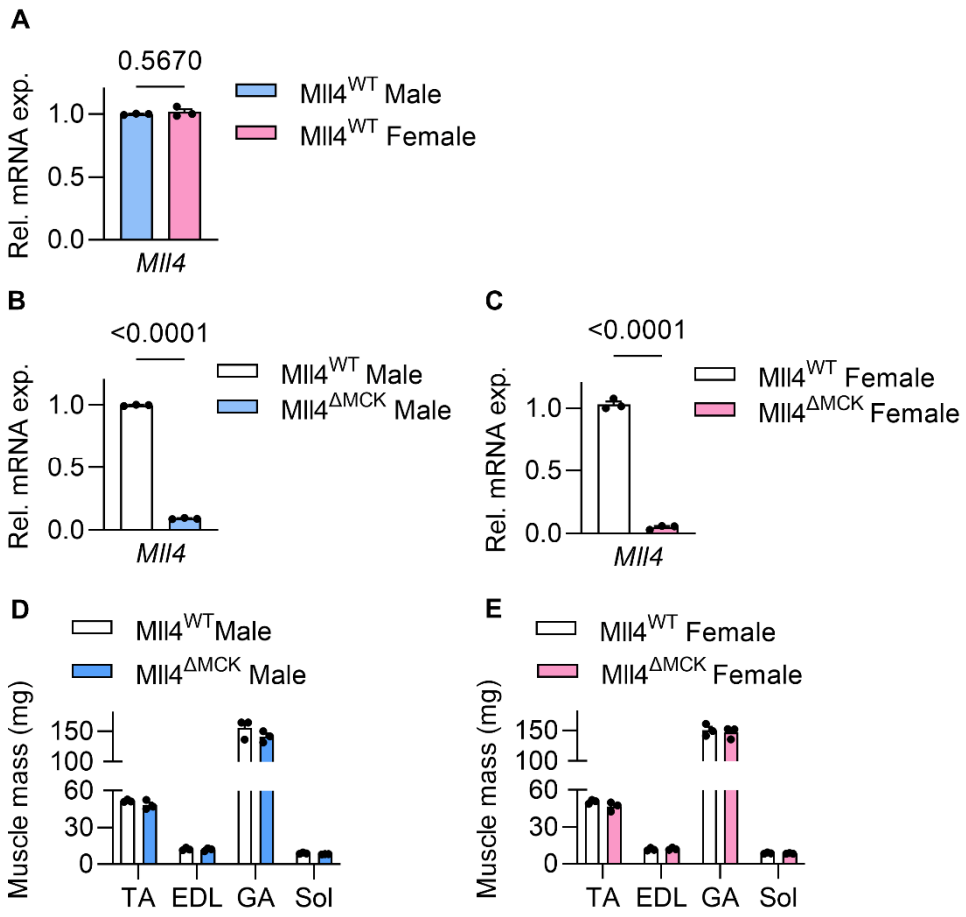
A
0.5670
Rel. mRNA exp.
1.0
0.5
0.0
Mll4
Mll4WT Male
Mll4WT Female
B
<0.0001
Rel. mRNA exp.
1.0
0.5
0.0
Mll4
Mll4WT Male
Mll4ΔMCK Male
C
<0.0001
Rel. mRNA exp.
1.0
0.5
0.0
Mll4
Mll4WT Female
Mll4ΔMCK Female
D
Mll4WTMale
Mll4ΔMCK Male
Muscle mass (mg)
150
100
60
30
0
TA EDL GA Sol
E
Mll4WT Female
Mll4ΔMCK Female
Muscle mass (mg)
150
100
60
30
0
TA EDL GA Sol

Figure 8. Fiber CSA and fiber type composition in adult male Mll4^{WT} and Mll4$^{\Delta MCK}$ mice. (A) Percentage of myofibers within each indicated range of CSA in TA muscle of Mll4$^{\Delta MCK}$ and Mll4^{WT} mice. n=3 mice for each genotype. (B) Representative image of soleus muscles immunolabeled with anti-MyHC1 (green) and anti-laminin (red). Scale bar, 500 μm. (C) The fiber number of whole TA muscles from Mll4^{WT} and Mll4$^{\Delta MCK}$ male mice. n=3 mice for each genotype. (D) The percentage of slow fiber among total fiber of soleus muscles from Mll4^{WT} and Mll4$^{\Delta MCK}$ male mice. n=3 mice for each genotype. Data are presented as mean ± SEM of biological replicates. Statistical analyses were performed using unpaired t-test with Welch's correction.

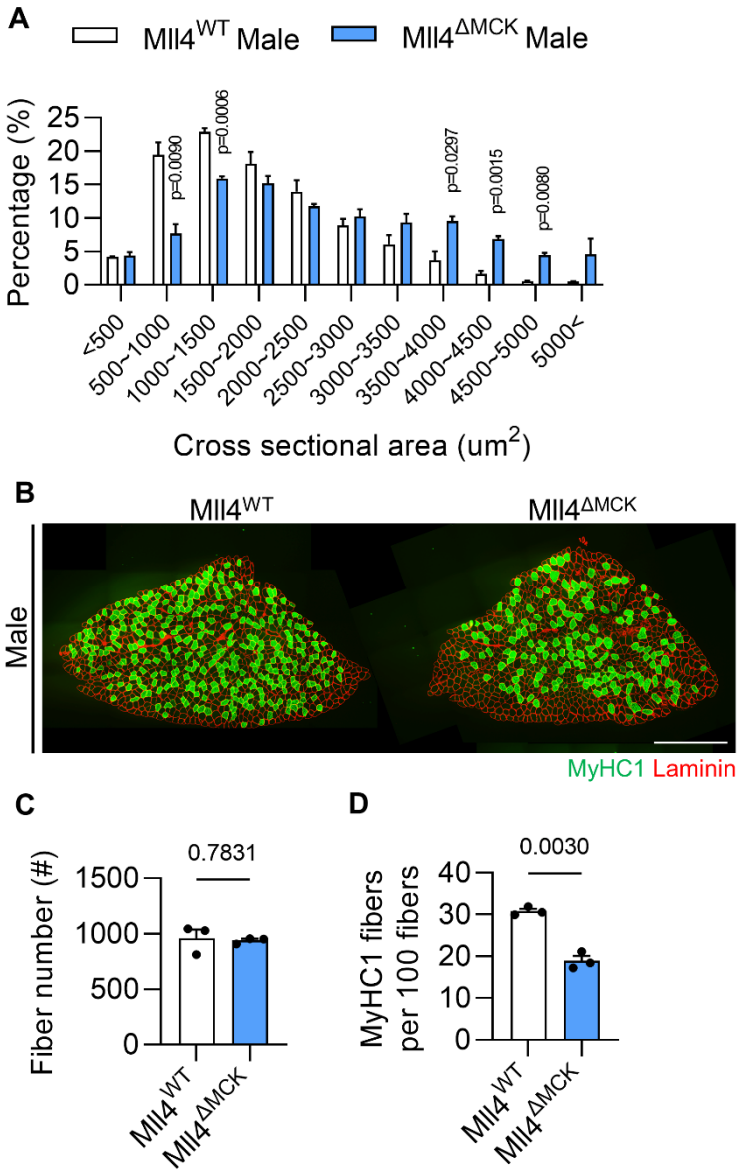
A
Mll4WT Male
Mll4ΔMCK Male
Percentage (%)
25
20
15
10
5
0
p=0.0090
p=0.0006
p=0.0297
p=0.0015
p=0.0080
<500
500~1000
1000~1500
1500~2000
2000~2500
2500~3000
3000~3500
3500~4000
4000~4500
4500~5000
5000<
Cross sectional area (um2)
B
Mll4WT
Mll4ΔMCK
Male
MyHC1 Laminin
C
Fiber number (#)
1500
1000
500
0
0.7831
Mll4WT
Mll4ΔMCK
D
MyHC1 fibers per 100 fibers
40
30
20
10
0
0.0030
Mll4WT
Mll4ΔMCK

Figure 9. Fiber CSA and fiber type composition in adult female Mll4^{WT} and Mll4$^{\Delta MCK}$ mice. (A) Percentage of myofibers within each indicated range of CSA in TA muscle of Mll4$^{\Delta MCK}$ and Mll4^{WT} mice. n=3 mice for each genotype. (B) Representative image of soleus muscles immunolabeled with anti-MyHC1 (green) and anti-laminin (red). Scale bar, 500 μm. (C) The fiber number of whole TA muscles from Mll4^{WT} and Mll4$^{\Delta MCK}$ female mice. n=3 mice for each genotype. (D) The percentage of slow fiber among total fiber of soleus muscles from Mll4^{WT} and Mll4$^{\Delta MCK}$ female mice. n=3 mice for each genotype. Data are presented as mean ± SEM of biological replicates. Statistical analyses were performed using unpaired t-test with Welch's correction.

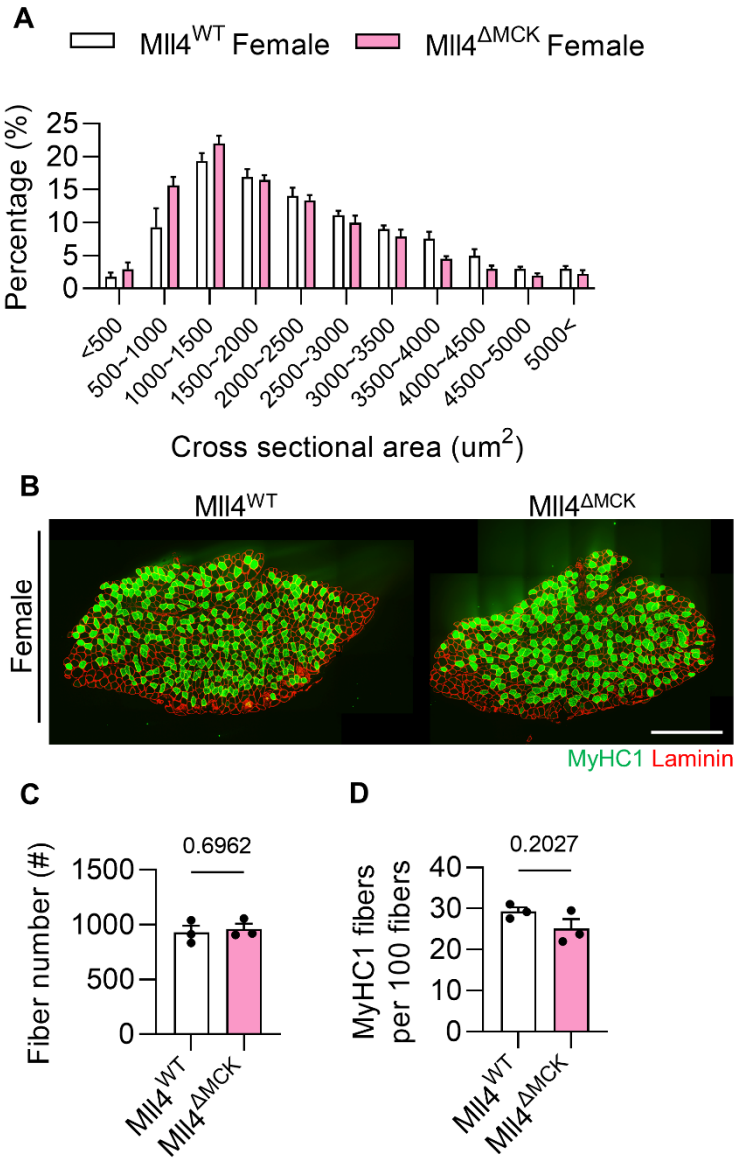
A
Mll4WT Female
Mll4ΔMCK Female
Percentage (%)
25
20
15
10
5
0
<500
500~1000
1000~1500
1500~2000
2000~2500
2500~3000
3000~3500
3500~4000
4000~4500
4500~5000
5000<
Cross sectional area (um2)
B
Mll4WT
Mll4ΔMCK
Female
MyHC1 Laminin
C
Fiber number (#)
1500
1000
500
0
0.6962
Mll4WT
Mll4ΔMCK
D
MyHC1 fibers per 100 fibers
40
30
20
10
0
0.2027
Mll4WT
Mll4ΔMCK

MuSC depletion in adult Mll4$^{\Delta MCK}$ mice

Unexpectedly, when isolating single myofibers to prove the ablation of Mll4 in Mll4$^{\Delta MCK}$ mice (Figure 10A), I observed that myofiber length was significantly shorter in both male and female Mll4$^{\Delta MCK}$ mice compared to those of controls (Figure 10B and 10E). Since shortened myofibers may be due to a reduced number of myonuclei (Cramer et al., 2020), I quantified myonuclear number, which was markedly decreased in Mll4$^{\Delta MCK}$ EDL myofibers compared to the controls (Figure 10C and 10F). To assess whether myonuclear density was also reduced, I calculated the ratio of myonuclear number to myofiber length. This analysis revealed a decrease in myonuclear density in Mll4$^{\Delta MCK}$ myofibers (Figure 10D and 10G).

During postnatal development in mice, myofiber length and myonuclear number increase rapidly through myoblast fusion until puberty and then become relatively stable at the adult stage when postnatal myogenesis ceases (White et al., 2010). Thus, reduced myonuclear density in adult Mll4$^{\Delta MCK}$ mice might be due to impaired myoblast fusion, defective MuSC differentiation, or even MuSC depletion. To address this issue, I first assessed the number of MuSCs in *Mll4*-deleted myofibers (Figure 11A). Intriguingly, Pax7^{+} MuSCs greatly decreased in the myofibers of both male and female 8-week-old Mll4$^{\Delta MCK}$ mice (Figure 11B-C). My data suggest that MuSC depletion in *Mll4*-lacking myofibers during postnatal myogenesis resulted in decreased myonuclei accretion and myofiber growth, and that *Mll4* in myofiber may play an important role in maintaining the MuSC population, irrespective of gender.

Figure 10. Altered myofiber phenotype of 8-week-old Mll4$^{\Delta MCK}$ mice in both sexes. (A) Representative image of the isolated single myofiber. DAPI staining was applied to visualize nuclei. Scale bar, 500 μm. (B, E) Myofiber length, (C, F) myonuclei accretion, and (D, G) myonuclear density were quantified. (B-G) n=3 mice for each genotype; >20 fibers per mouse was quantified. Data are presented as mean ± SEM of biological replicates. Statistical analyses were performed using unpaired t-test with Welch's correction.

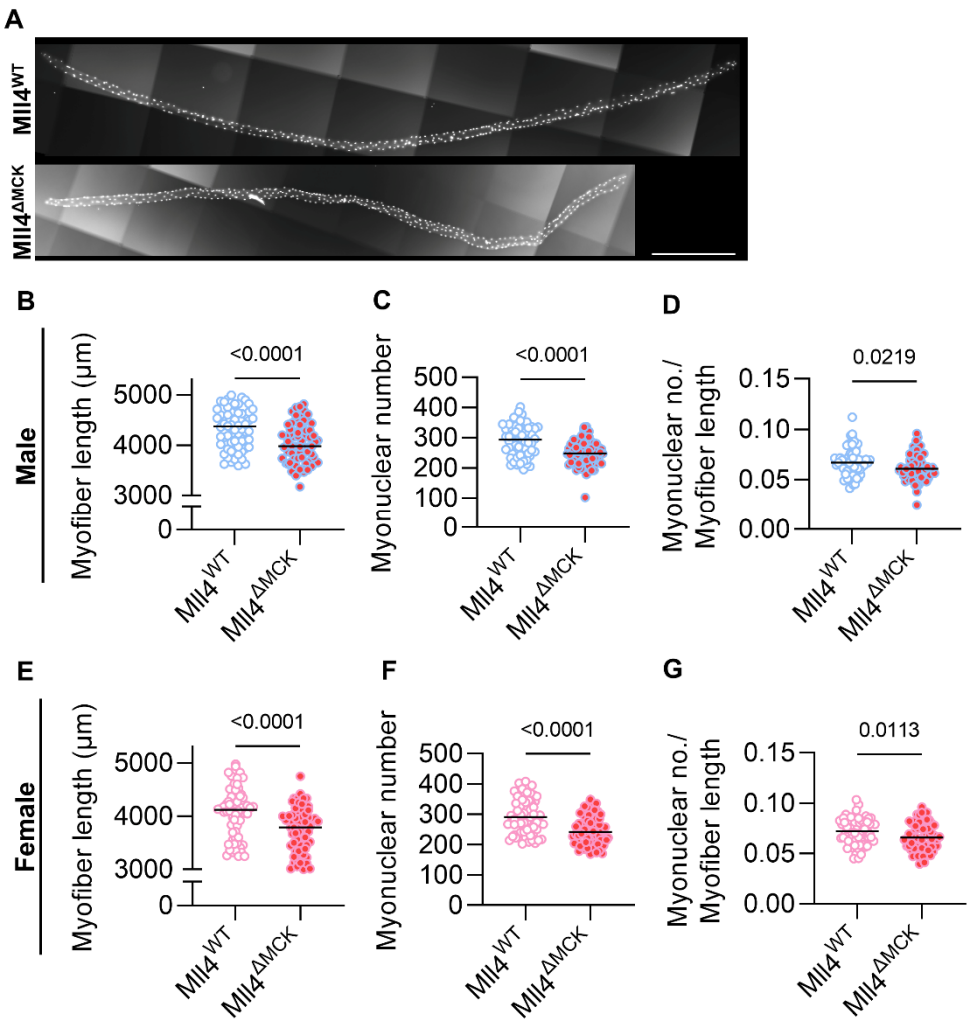
A
Mll4WT
Mll4ΔMCK
B
Male
Myofiber length (μm)
<0.0001
5000
4000
3000
0
Mll4WT
Mll4ΔMCK
C
Myonuclear number
<0.0001
500
400
300
200
100
0
Mll4WT
Mll4ΔMCK
D
Myonuclear no./ Myofiber length
0.0219
0.15
0.10
0.05
0.00
Mll4WT
Mll4ΔMCK
E
Female
Myofiber length (μm)
<0.0001
5000
4000
3000
0
Mll4WT
Mll4ΔMCK
F
Myonuclear number
<0.0001
500
400
300
200
100
0
Mll4WT
Mll4ΔMCK
G
Myonuclear no./ Myofiber length
0.0113
0.15
0.10
0.05
0.00
Mll4WT
Mll4ΔMCK

Figure 11. Reduced Pax7-positive MuSC number of 8-week-old Mll4$^{\Delta MCK}$ mice. (A) Immunocytochemistry of isolated myofibers of 4-week-old Mll4$^{\Delta MCK}$ and Mll4^{WT} mice with DAPI (blue) and anti-Pax7 (red). MuSCs are marked with arrowheads. Scale bars, 100 μm. (B, C) Pax7^{+} MuSC number per fiber of Mll4^{WT} and Mll4$^{\Delta MCK}$ mice of both genders. (B, C) n=3 mice for each genotype; >20 fibers per mouse was quantified. Data are presented as mean ± SEM of biological replicates. Statistical analyses were performed using unpaired t-test with Welch's correction.

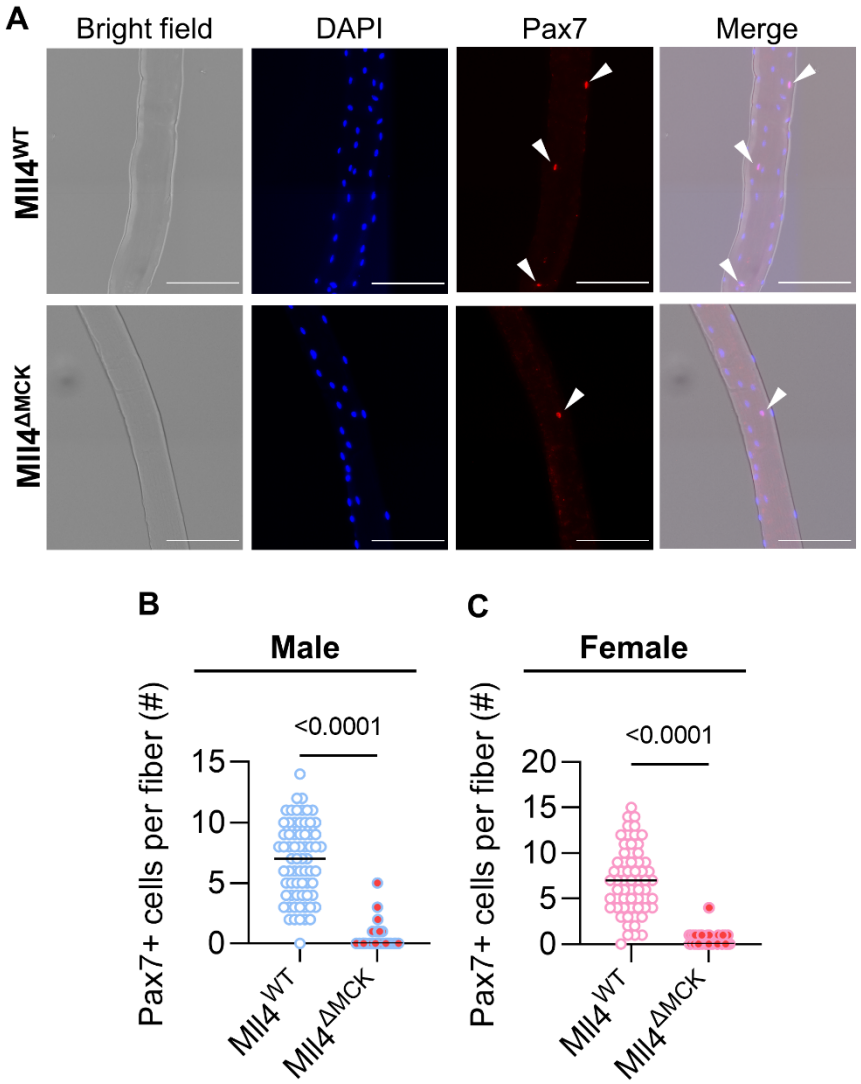
A
Bright field
DAPI
Pax7
Merge
Mll4WT
Mll4ΔMCK
B
Male
<0.0001
Pax7+ cells per fiber (#)
15
10
5
0
Mll4WT
Mll4ΔMCK
C
Female
<0.0001
Pax7+ cells per fiber (#)
20
15
10
5
0
Mll4WT
Mll4ΔMCK

MuSC depletion in *Mll4* deleted muscle during postnatal muscle growth

MuSCs that have actively proliferated during the juvenile stage enter a quiescent state at puberty to establish a reserve stem cell pool in adult muscles (Kim et al., 2016). To investigate if the deletion of Mll4 in myofibers affects MuSC number during postnatal myogenesis, I conducted a histological analysis to quantify Pax7-positive cells in TA muscles during and after postnatal myogenesis. Considering that MCK-Cre mediated ablation of *Mll4* occurs after 7 days of birth (Liu et al., 2020), 0-week-old perinatal muscles were expected to have comparable MuSC numbers between $Mll4^{WT}$ and $Mll4^{\Delta MCK}$ muscles. The number of MuSCs remained consistent between the control and $Mll4^{\Delta MCK}$ muscles until 2 weeks of age (Figure 12A). However, a decrease of $Pax7^{+}$ MuSCs was prominent in the pubertal 4-week-old $Mll4^{\Delta MCK}$ TA muscle, with a further decline noted in the 8-week-old muscle (Figure 12A-B). This indicates that the deletion of myofiber-specific *Mll4* disrupts the MuSC number during postnatal myogenesis, resulting in a depletion of the population in adult muscles.

TA and EDL muscles primarily consist of fast-twitch type 2 fibers (Augusto et al., 2004). To examine if MuSC depletion occurs in slow-twitch type 1 fiber-rich muscles, the soleus muscle was analyzed. Undoubtedly, the Pax7-positive MuSC number was reduced in the pubertal 4-week-old muscles and further diminished in the adult 8-week-old soleus muscles of $Mll4^{\Delta MCK}$ mice (Figure 12C-D).

Figure 12. MuSC is depleted in 4-week-old Mll4$^{\Delta MCK}$ muscles. (A) Pax7+ MuSC number per 100 fibers was quantified in TA muscles of 0, 2, 4, and 8-week-old Mll4$^{\Delta MCK}$ and littermate control mice. (B) Immunohistochemistry on TA muscle section with DAPI (blue), anti-laminin (green), and anti-Pax7 (red). Scale bars, 20 μm. (C) Pax7+ MuSC number per 100 fibers was quantified in soleus muscles of 4 and 8-week-old Mll4$^{\Delta MCK}$ and littermate control mice. (D) Immunohistochemistry on soleus muscle section with DAPI (blue), anti-laminin (green), and anti-Pax7 (red). Scale bars, 20 μm. (A, C) n=3-4 mice for each genotype. Data are presented as mean ± SEM of biological replicates. Statistical analyses were performed using unpaired t-test with Welch's correction.

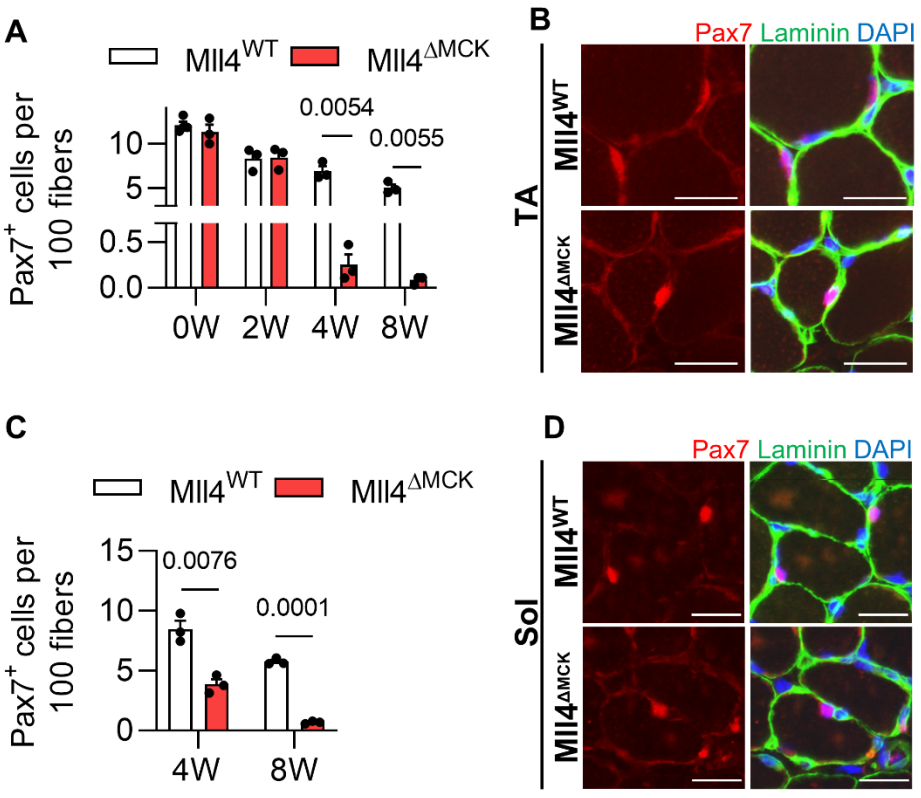
A
Mll4WT
Mll4ΔMCK
Pax7+ cells per 100 fibers
10
5
0.5
0.0
0.0054
0.0055
0W
2W
4W
8W
B
Pax7 Laminin DAPI
TA
Mll4WT
Mll4ΔMCK
C
Mll4WT
Mll4ΔMCK
Pax7+ cells per 100 fibers
15
10
5
0
0.0076
0.0001
4W
8W
D
Pax7 Laminin DAPI
Sol
Mll4WT
Mll4ΔMCK

During puberty, cycling MuSCs exit the cell cycle and contribute to quiescent MuSC populations (Kim et al., 2016). To test if the reduced MuSC in Mll4$^{\Delta MCK}$ mice was due to impaired cell cycle exit in cycling pubertal MuSCs, I quantified Ki67-positive MuSCs in the 4-week-old Mll4$^{\Delta MCK}$ mice. Compared to the control, Mll4$^{\Delta MCK}$ mice showed a twofold increase in proliferating Ki67^{+}Pax7^{+} MuSCs (Figure 13A-B). To investigate if these proliferating MuSCs enter the differentiation state, I isolated MuSCs via cytometry (Figure 14A-B) and quantified MyoD-positive MuSCs. To clarify, cells that show low Pax7 expression coupled with high MyoD expression were classified as 'MyoD-positive' cells. Compared to the Mll4^{WT} mice, Mll4$^{\Delta MCK}$ mice showed an increase in MyoD-positive MuSCs (Figure 15A-B). Furthermore, to label cycling MuSCs, EdU was treated for 2 consecutive days before isolating MuSCs (Figure 15C). Notably, the number of MyoD-positive cells also increased among cycling MuSCs (Edu^{+}Pax7^{+}) in Mll4$^{\Delta MCK}$ mice (Figure 15D). This indicates that while normal MuSCs exit the cell cycle and enter a quiescent state during puberty, MuSCs in Mll4$^{\Delta MCK}$ mice maintain their cell cycle and differentiate into committed myoblasts. Altogether, the deletion of Mll4 in myofibers leads to the loss of MuSCs during postnatal muscle growth.

Figure 13. Increased Ki67-positive cycling MuSCs in 4-week-old Mll4$^{\Delta MCK}$ muscles. (A) Immunohistochemistry on 4W TA muscle section with DAPI (blue), anti-Ki67 (green), and anti-Pax7 (red). Scale bars, 20 μm. (B) Pax7^{+}Ki67^{+} cell number per total Pax7^{+} cells of 4W TA muscle. N=3-4 mice for each genotype. Data are presented as mean ± SEM of biological replicates. Statistical analyses were performed using unpaired t-test with Welch's correction.

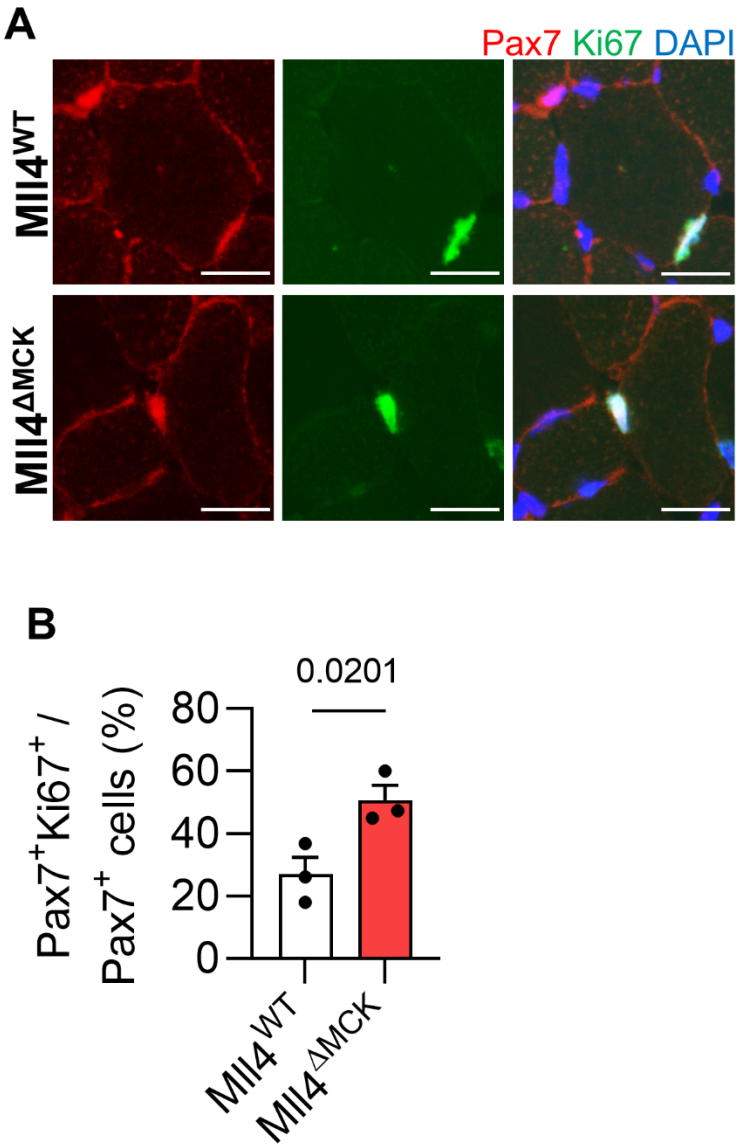
A
Pax7 Ki67 DAPI
MII4WT
MII4ΔMCK
B
0.0201
Pax7+Ki67+ / Pax7+ cells (%)
80
60
40
20
0
MII4WT
MII4ΔMCK

Figure 14. Flow cytometry of cell surface markers of limb muscles to isolate MuSCs. (A-B) Gating strategies for isolating MuSCs in Mll4$^{\Delta MCK}$ muscles with control muscles. Each figure is representative of n = 3 mice. Data are presented as mean ± SEM of biological replicates. Statistical analyses were performed using unpaired t-test with Welch's correction.

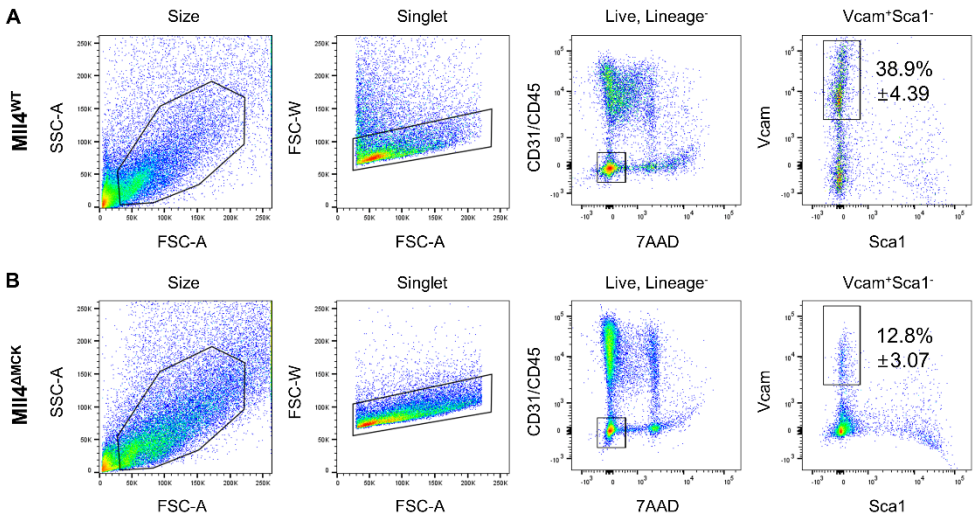
A
Mll4WT
Size
SSC-A
FSC-A
Singlet
FSC-W
FSC-A
Live, Lineage-
CD31/CD45
7AAD
Vcam+Sca1-
Vcam
Sca1
38.9%
±4.39
B
Mll4ΔMCK
Size
SSC-A
FSC-A
Singlet
FSC-W
FSC-A
Live, Lineage-
CD31/CD45
7AAD
Vcam+Sca1-
Vcam
Sca1
12.8%
±3.07

Figure 15. MuSC depletion due to increased number of differentiating myoblasts in 4-week-old Mll4$^{\Delta MCK}$ muscles. (A) Immunocytochemistry of sorted MuSCs with DAPI (blue), anti-Pax7 (red), anti-MyoD (green), and EdU (white – pseudo color for Alexa Fluor 647). MyoD^{+} cells and EdU^{+} cells are marked with arrowheads and sharps, respectively. Scale bars, 20 μm. For enlarged images, Scale bars represent 10 μm. (B) MyoD^{+} cell number per total Pax7^{+} cells. (C) Schematic diagram of EdU treatment. (D) MyoD^{+} cell number per EdU^{+}Pax7^{+} cells. (B, D) n=3-4 mice for each genotype; >200 sorted MuSCs per mouse were quantified. Data are presented as mean ± SEM of biological replicates. Statistical analyses were performed using unpaired t-test with Welch's correction.

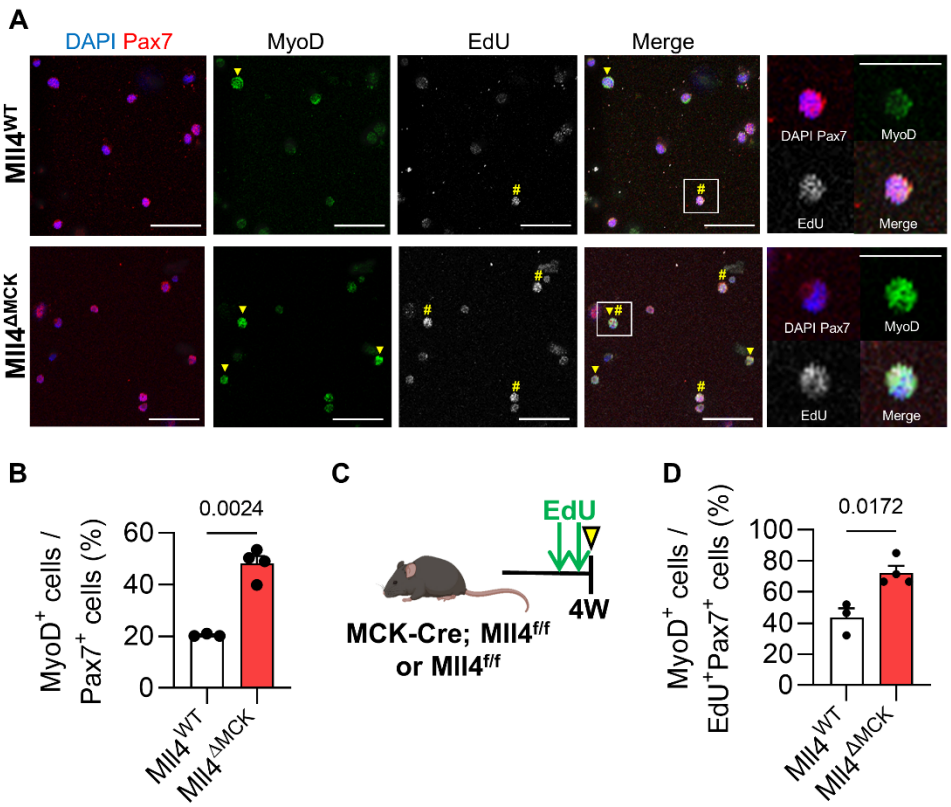
A
DAPI Pax7
MyoD
EdU
Merge
MII4WT
MII4ΔMCK
DAPI Pax7
MyoD
EdU
Merge
B
0.0024
MyoD+ cells / Pax7+ cells (%)
60
40
20
0
MII4 WT
MII4 ΔMCK
C
EdU
4W
MCK-Cre; MII4f/f
or MII4f/f
D
0.0172
MyoD+ cells / EdU+Pax7+ cells (%)
100
80
60
40
20
0
MII4 WT
MII4 ΔMCK

Deletion of Mll4 in adult myofibers does not alter muscle CSA and fiber type composition

Following postnatal myogenesis, the adult muscle tissue reaches a steady state characterized by the cessation of myofiber growth and the entry of MuSCs into a quiescent phase. To investigate if induced ablation of *Mll4* in muscles after postnatal myogenesis would affect myofiber maintenance, I examined muscle features such as CSA distribution and fiber type composition of *Mll4* ablated adult muscles. Adult $HSA^{MerCreMer/+}$; $Mll4^{f/f}$ mice ($Mll4^{\Delta HSA}$) were treated with tamoxifen for consecutive 5 days to induce deletion of the *Mll4* gene in myofibers (Figure 16A). This resulted in the ablation of the *Mll4* gene in the myofibers of $Mll4^{\Delta HSA}$ mice after 2 weeks of tamoxifen administration (Figure 16B). The histological analysis showed that CSA distribution, fiber number, and fast-twitch (MyHC2x) fiber composition in the TA muscles of $Mll4^{\Delta HSA}$ mice did not change following 2 weeks (Figure 17A-C and 18A) and even 4 weeks (Figure 19A-C and 20A) of *Mll4* ablation, compared to the control mice. Similarly, in the soleus muscle, the composition of slow-twitch (MyHC1) fibers also remained unchanged after both 2 weeks (Figure 17D-E and 18A) and 4 weeks (Figure 19D-E and 20A) of *Mll4* ablation in $Mll4^{\Delta HSA}$ mice. This indicates that the induced deletion of *Mll4* in adult muscles does not affect myofiber maintenance and intracellular features such as fiber CSA and fiber type composition regardless of gender.

Figure 16. Schematic diagram of mouse preparation. (A) HSA-Cre^{ER}; Mll4$^{f/f}$ or Mll4$^{f/f}$ mice were treated with tamoxifen to ablate Mll4 in myofibers. Mice were sacrificed after 2 weeks (+2W Mll4$^{\Delta HSA}$) and 4 weeks (+4W Mll4$^{\Delta HSA}$) of tamoxifen administration. (B) Deletion of Mll4 was confirmed in +2W Mll4$^{\Delta HSA}$ myofibers via qRT-PCR. n=3 mice for each genotype. Data are presented as mean ± SEM of biological replicates. Statistical analyses were performed using unpaired t-test with Welch's correction.

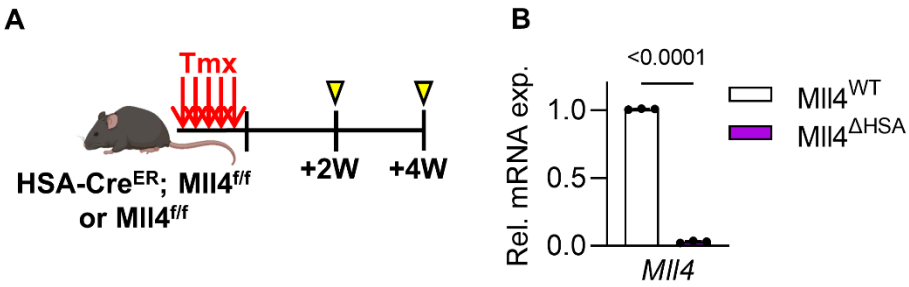
A
Tmx
+2W
+4W
HSA-Cre^ER; Mll4^f/f
or Mll4^f/f
B
<0.0001
Rel. mRNA exp.
1.0
0.5
0.0
Mll4
Mll4^WT
Mll4^ΔHSA

Figure 17. Ablation of Mll4 in adult muscles does not alter muscle CSA and fiber type composition. (A) Percentage of myofibers within each indicated range of CSA, (B) gross fiber number, and (C) percentage of MyHC2x fibers in TA muscle of $Mll4^{WT}$ and +2W $Mll4^{\Delta HSA}$ mice. (D) Gross fiber number and (E) percentage of MyHC1 fibers in soleus muscle of $Mll4^{WT}$ and $Mll4^{\Delta HSA}$ mice. (C-G) n=3 mice for each genotype. Data are presented as mean ± SEM of biological replicates. Statistical analyses were performed using unpaired t-test with Welch's correction.

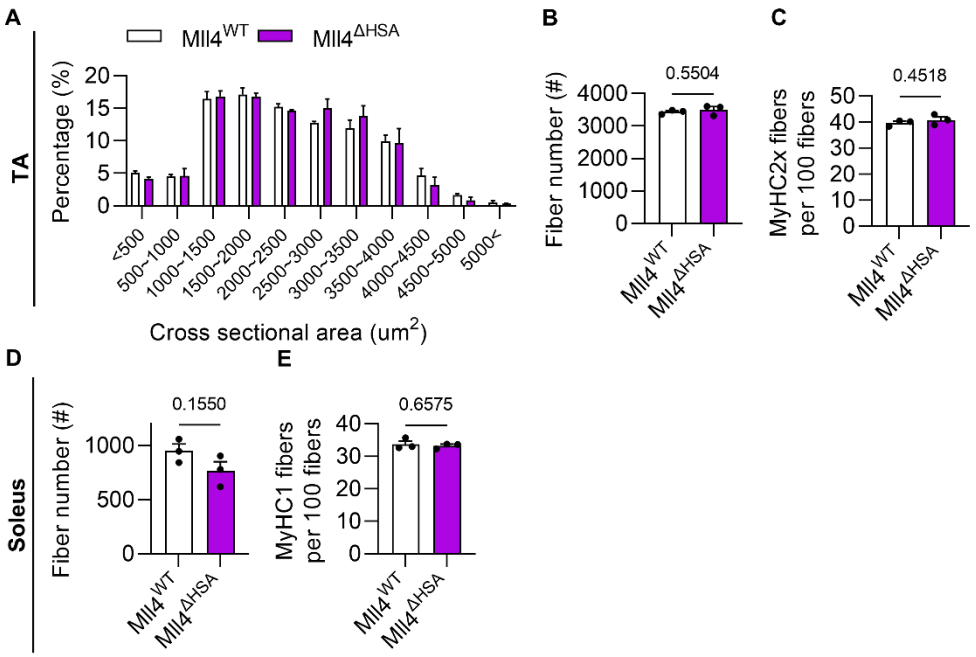
A
TA
Mll4WT
Mll4ΔHSA
Percentage (%)
20
15
10
5
0
<500
500~1000
1000~1500
1500~2000
2000~2500
2500~3000
3000~3500
3500~4000
4000~4500
4500~5000
5000<
Cross sectional area (um2)
B
Fiber number (#)
4000
3000
2000
1000
0
0.5504
Mll4WT
Mll4ΔHSA
C
MyHC2x fibers per 100 fibers
50
40
30
20
10
0
0.4518
Mll4WT
Mll4ΔHSA
D
Soleus
Fiber number (#)
1000
500
0
0.1550
Mll4WT
Mll4ΔHSA
E
MyHC1 fibers per 100 fibers
40
30
20
10
0
0.6575
Mll4WT
Mll4ΔHSA

Figure 18. The fiber area and fiber type composition following 2 weeks of Mll4 deletion. (A, B) Representative image of TA and soleus muscle. TA muscles were labeled with anti-MyHC2x (green) and anti-laminin (red). Soleus muscles were labeled with anti-MyHC1 (green) and anti-laminin (red). Scale bars, 500 μm.

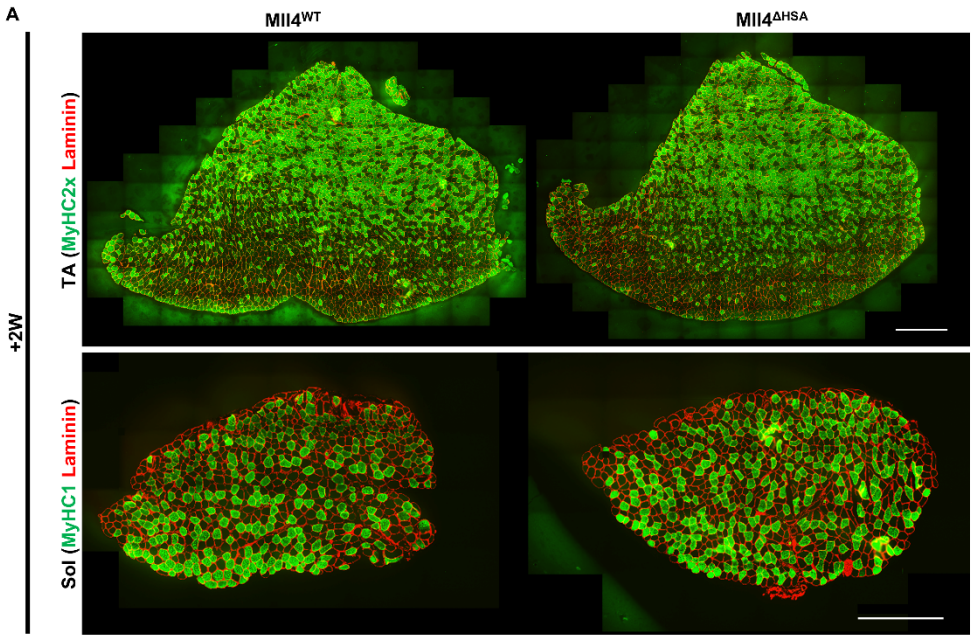
A
Mll4WT
Mll4ΔHSA
+2W
TA (MyHC2x Laminin)
Sol (MyHC1 Laminin)

Figure 19. Mll4$^{\Delta HSA}$ mice after a prolonged period after Mll4 deletion exhibit normal myofiber characteristics. (A) Percentage of myofibers within each indicated range of CSA, (B) gross fiber number, and (C) percentage of MyHC2x fibers in TA muscle of Mll4^{WT} and +4W Mll4$^{\Delta HSA}$ mice. (D) Gross fiber number (E) and percentage of MyHC1 fibers in soleus muscle of Mll4^{WT} and +4W Mll4$^{\Delta HSA}$ mice. (H-L) n=3 mice for each genotype. Data are presented as mean ± SEM of biological replicates. Statistical analyses were performed using unpaired t-test with Welch's correction.

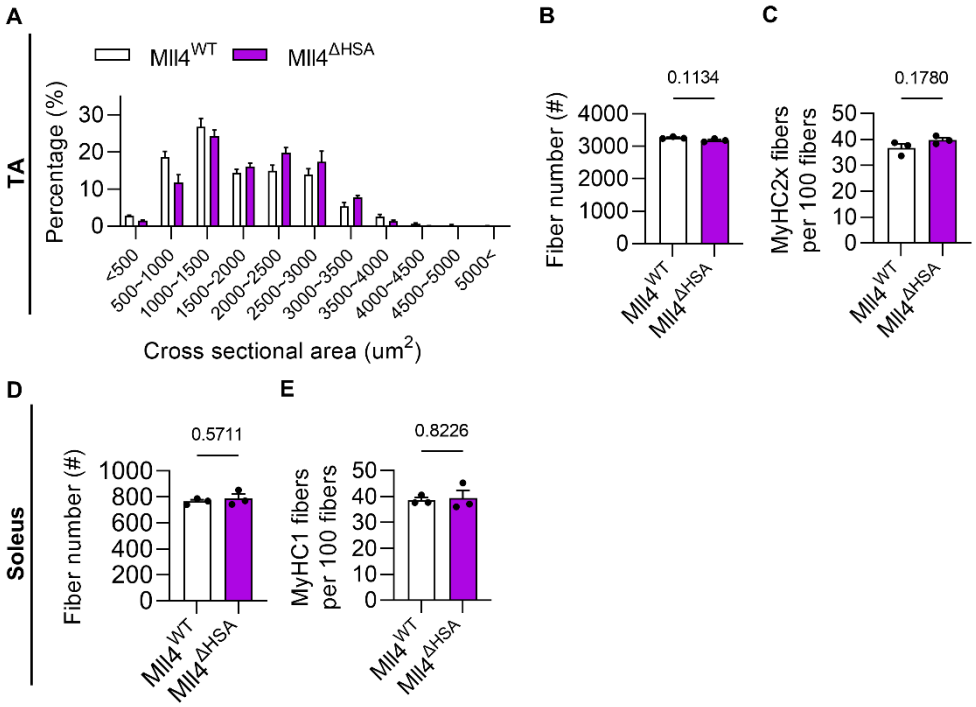
A
TA
Mll4WT
Mll4ΔHSA
Percentage (%)
30
20
10
0
<500
500~1000
1000~1500
1500~2000
2000~2500
2500~3000
3000~3500
3500~4000
4000~4500
4500~5000
5000<
Cross sectional area (um2)
B
0.1134
Fiber number (#)
4000
3000
2000
1000
0
Mll4WT
Mll4ΔHSA
C
0.1780
MyHC2x fibers per 100 fibers
50
40
30
20
10
0
Mll4WT
Mll4ΔHSA
D
Soleus
0.5711
Fiber number (#)
1000
800
600
400
200
0
Mll4WT
Mll4ΔHSA
E
0.8226
MyHC1 fibers per 100 fibers
50
40
30
20
10
0
Mll4WT
Mll4ΔHSA

Figure 20. The fiber area and fiber type composition following 4 weeks of Mll4 deletion. (A) Representative image of TA and soleus muscle. TA muscles were labeled with anti-MyHC2x (green) and anti-laminin (red). Soleus muscles were labeled with anti-MyHC1 (green) and anti-laminin (red). Scale bars, 500 μm.

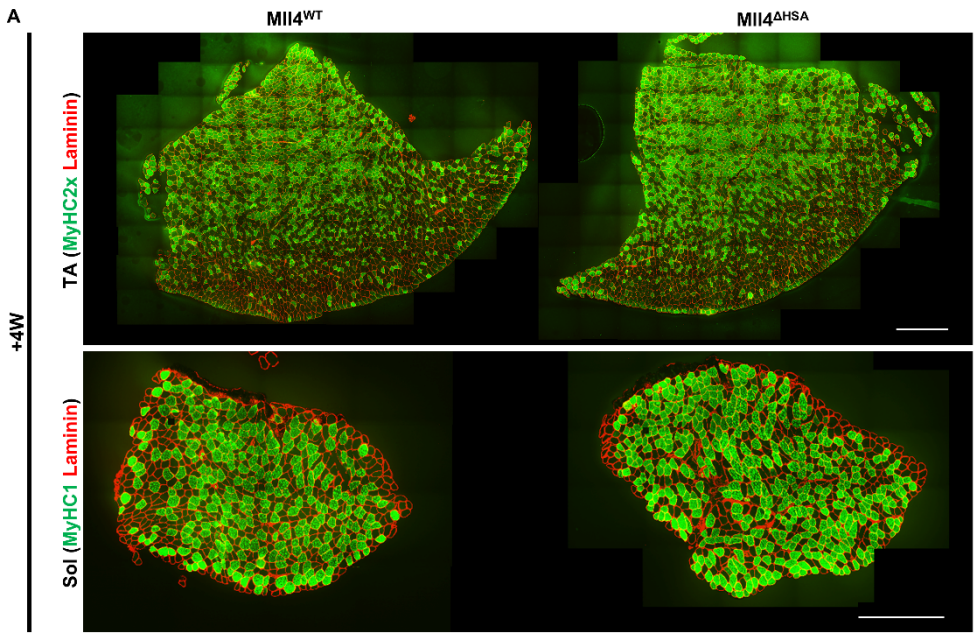
A
Mll4WT
Mll4ΔHSA
+4W
TA (MyHC2x Laminin)
Sol (MyHC1 Laminin)

Mll4 deletion in myofibers does not affect exercise capacity

Since MLL4 functions as an enhancer activator (Lee et al., 2013), its deletion may disrupt various gene transcription processes. Although the deletion of Mll4 in adult muscles does not impact myofiber characteristics such as CSA and fiber type composition, I investigated whether the deletion affects exercise capacity. To test this, tamoxifen-treated mice were accustomed to chronic exercise training for 5 weeks (hereafter, $Mll4^{WT\text{-}EX}$ and $Mll4^{\Delta HSA\text{-}EX}$) (Figure 21A). The protocol of the chronic exercise provides prolonged contractions of muscles, promoting adaptations such as increased muscle mass while minimizing exercise-induced muscle damage (Seo et al., 2021). In TA muscles, CSA distribution and fast fiber composition remained consistent between $Mll4^{WT\text{-}EX}$ and $Mll4^{\Delta HSA\text{-}EX}$ mice (Figure 22A-D). In addition, slow fiber composition was unchanged in $Mll4^{\Delta HSA\text{-}EX}$ soleus muscle (Figure 23A-C).

To assess whether exercise capacity was affected by Mll4 deletion, I measured grip strength and endurance running capability. In line with the observed similarity in CSA and fiber type composition, $Mll4^{\Delta HSA\text{-}EX}$ mice showed comparable grip strength (Figure 24A) and endurance running capability (Figure 24B-C) relative to the control group. To investigate whether the expression of genes related to fiber type and metabolism was altered in $Mll4^{\Delta HSA\text{-}EX}$ mice, I conducted qRT-PCR analyses. Transcriptional profiling revealed that before exercise training, the genes were generally downregulated in $Mll4^{\Delta HSA}$ mice (figure 25A-B). Notably, no particular gene exhibited higher expression levels that could induce a shift in fiber type composition or metabolic activity. After 5 weeks of chronic exercise, the expression of genes related to fiber type and metabolism of $Mll4^{\Delta HSA\text{-}EX}$ mice also showed

overall downregulation, with the exception that certain slow-twitch muscle genes were marginally upregulated (Figure 25C). Collectively, the results suggest that the induced knockout of *Mll4* in myofibers at the adult stage does not influence exercise capacity or muscle characteristics, such as CSA and fiber type composition, even after physiological exercise stimulation.

Figure 21. Schematic diagram of mouse exercise training and preparation. (A) HSA-Cre^{ER}; Mll4$^{f/f}$ or Mll4$^{f/f}$ mice were treated with tamoxifen to ablate Mll4 in myofibers. After 4 weeks, mice underwent a 5-week chronic exercise training protocol. Endurance exercise capacity was evaluated on the final day of training, while grip strength was measured the following day prior to sacrifice.

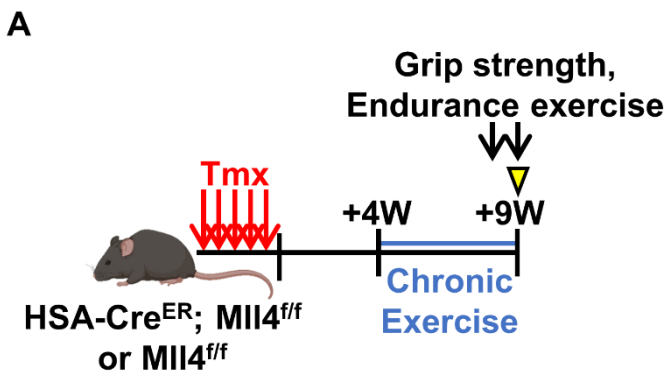
A
Grip strength,
Endurance exercise
Tmx
+4W
+9W
Chronic
Exercise
HSA-Cre^ER; Mll4^f/f
or Mll4^f/f

Figure 22. Normal muscle feature in myofiber-*Mll4* deleted TA muscles after chronic exercise. (A) Representative image of TA and soleus muscle. Anti-MyHC2x (green) and anti-laminin (red). Scale bars, 500 μm.(B) Percentage of myofibers within each indicated range of CSA, (C) gross fiber number, and (D) percentage of MyHC2x fibers in TA muscle of $Mll4^{\Delta WT\text{-}EX}$ and $Mll4^{\Delta HSA\text{-}EX}$ mice. (B-D) n=6 mice for each genotype. Data are presented as mean ± SEM of biological replicates. Statistical analyses were performed using unpaired t-test with Welch's correction.

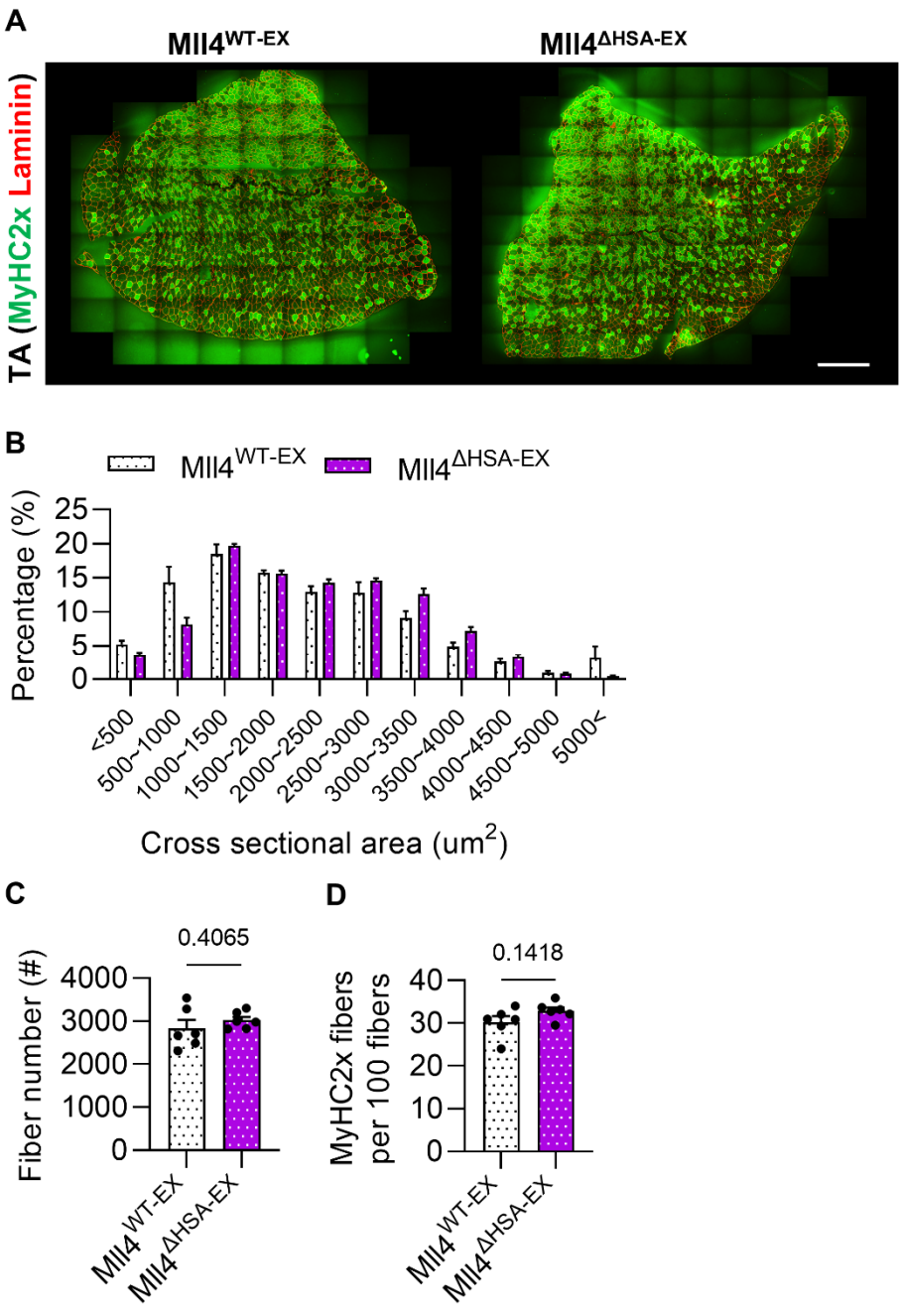
A
Mll4WT-EX
Mll4ΔHSA-EX
TA (MyHC2x Laminin)
B
Mll4WT-EX
Mll4ΔHSA-EX
Percentage (%)
25
20
15
10
5
0
<500
500~1000
1000~1500
1500~2000
2000~2500
2500~3000
3000~3500
3500~4000
4000~4500
4500~5000
5000<
Cross sectional area (um2)
C
0.4065
Fiber number (#)
4000
3000
2000
1000
0
Mll4WT-EX
Mll4ΔHSA-EX
D
0.1418
MyHC2x fibers per 100 fibers
40
30
20
10
0
Mll4WT-EX
Mll4ΔHSA-EX

Figure 23. Myofiber type does not alter in soleus muscles of Mll4$^{\Delta HSA\text{-}EX}$ mice after exercise. (A) Representative image of the soleus muscle. Anti-MyHC1 (green) and anti-laminin (red). Scale bars, 500 μm. (B) Gross fiber number and (C) percentage of MyHC1 fibers in soleus muscle of Mll4$^{\Delta WT\text{-}EX}$ and Mll4$^{\Delta HSA\text{-}EX}$ mice. (B-C) n=6 mice for each genotype. Data are presented as mean ± SEM of biological replicates. Statistical analyses were performed using unpaired t-test with Welch's correction.

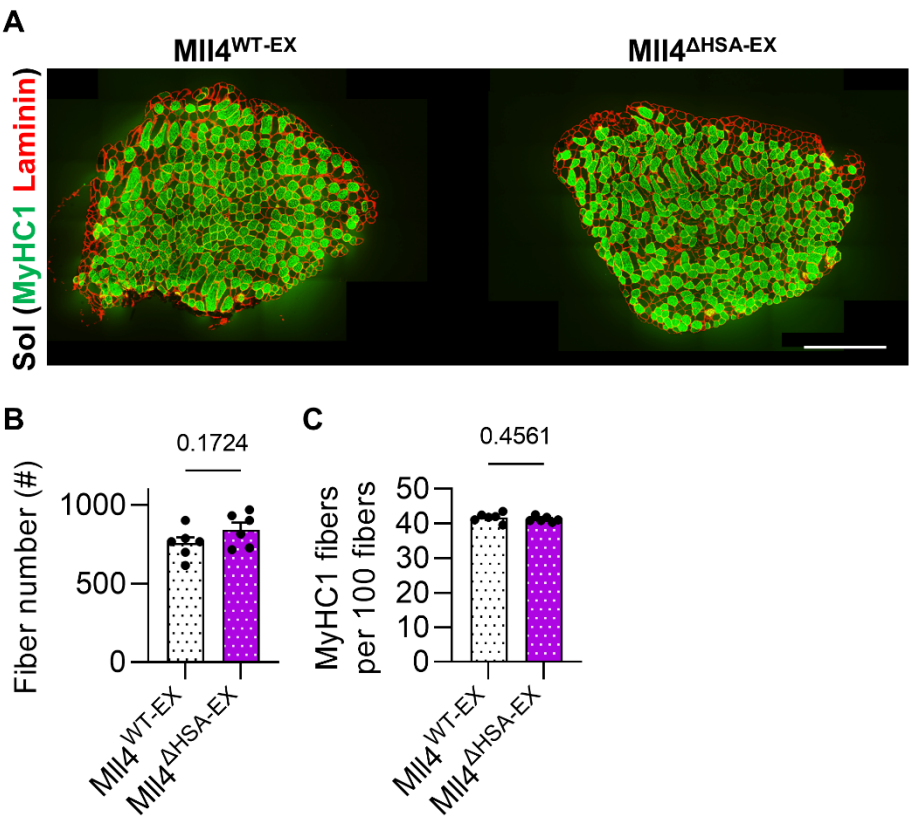
A
Mll4WT-EX
Mll4ΔHSA-EX
Sol (MyHC1 Laminin)
B
0.1724
Fiber number (#)
1000
500
0
Mll4 WT-EX
Mll4 ΔHSA-EX
C
0.4561
MyHC1 fibers per 100 fibers
50
40
30
20
10
0
Mll4 WT-EX
Mll4 ΔHSA-EX

Figure 24. Normal exercise capacity of myofiber-specific *Mll4* deleted muscles. (A) The measurement values of grip strength (N/g) of Mll4$^{\Delta WT\text{-}EX}$ and Mll4$^{\Delta HSA\text{-}EX}$ mice. Grip strength (N) was normalized to body weight (g). (B, C) The measurement values of endurance running test. Total running time (min) (I) and total running distance (m) (J) of Mll4$^{\Delta WT\text{-}EX}$ and Mll4$^{\Delta HSA\text{-}EX}$ mice. (A-C) n=6 mice for each genotype. Data are presented as mean ± SEM of biological replicates. Statistical analyses were performed using unpaired t-test with Welch's correction.

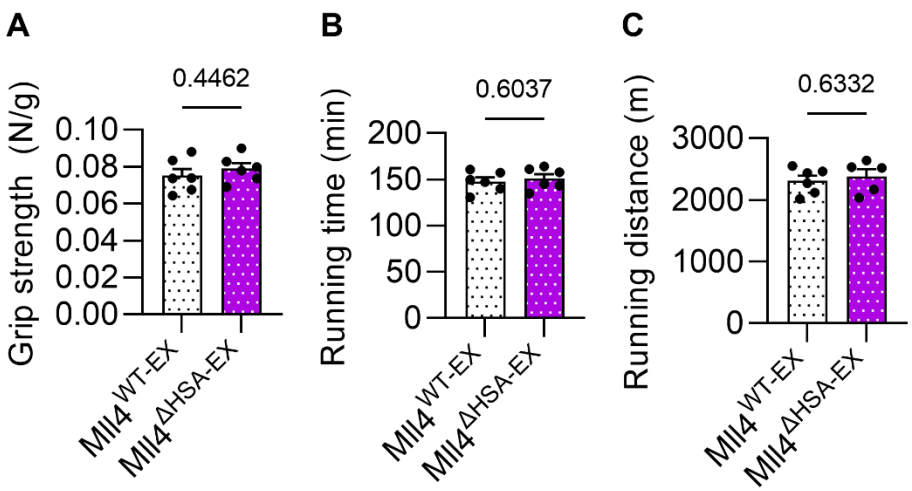
A
B
C
0.4462
0.6037
0.6332
Grip strength (N/g)
Running time (min)
Running distance (m)
0.10
0.08
0.06
0.04
0.02
0.00
200
150
100
50
0
3000
2000
1000
0
Mll4 WT-EX
Mll4 ΔHSA-EX

Figure 25. Gene expression related to fiber type and metabolism in *Mll4*-ablated muscle under various conditions. (A, B, C) Normalized expression of representative genes of slow-twitch fiber, fast-twitch fiber, glucose metabolism, and fat metabolism in TA muscle from $Mll4^{\Delta HSA}$ +2W (A), $Mll4^{\Delta HSA}$ +4W (B), and $Mll4^{\Delta HSA\text{-}EX}$ (C) mice. (A, B) n=3 mice for each genotype. (C) n=6 mice for each genotype. (A, B, and C) Data are presented as mean ± SEM of biological replicates. Statistical analyses were performed using unpaired t-test with Welch's correction.

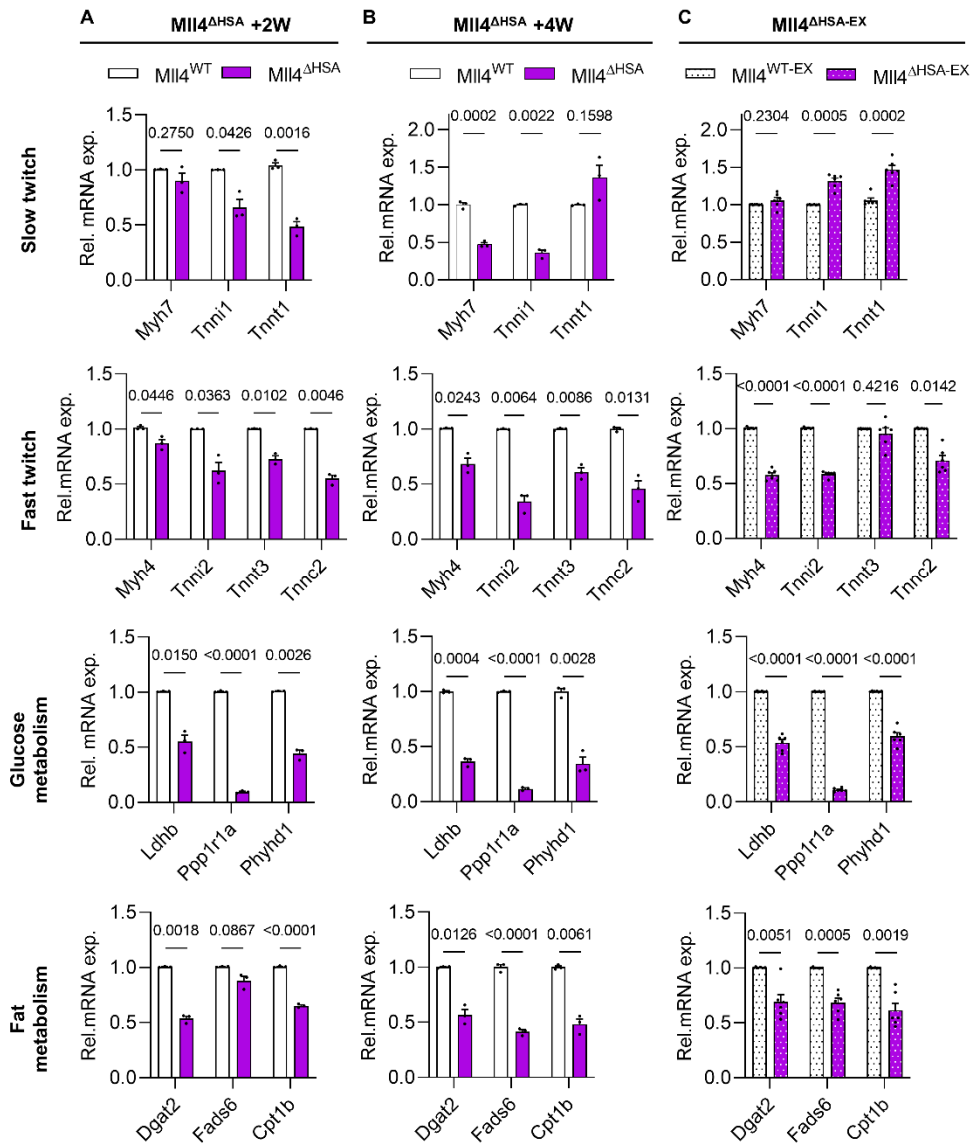
A
Mll4ΔHSA +2W
Mll4WT
Mll4ΔHSA
B
Mll4ΔHSA +4W
Mll4WT
Mll4ΔHSA
C
Mll4ΔHSA-EX
Mll4WT-EX
Mll4ΔHSA-EX
Slow twitch
Fast twitch
Glucose metabolism
Fat metabolism
Rel. mRNA exp.
Rel.mRNA exp.
0.2750 0.0426 0.0016
0.0002 0.0022 0.1598
0.2304 0.0005 0.0002
0.0446 0.0363 0.0102 0.0046
0.0243 0.0064 0.0086 0.0131
<0.0001 <0.0001 0.4216 0.0142
0.0150 <0.0001 0.0026
0.0004 <0.0001 0.0028
<0.0001 <0.0001 <0.0001
0.0018 0.0867 <0.0001
0.0126 <0.0001 0.0061
0.0051 0.0005 0.0019
Myh7
Tnni1
Tnnt1
Myh4
Tnni2
Tnnt3
Tnnc2
Ldhb
Ppp1r1a
Phyhd1
Dgat2
Fads6
Cpt1b

Loss of adult MuSCs in Mll4$^{\Delta HSA}$ mice

To investigate whether the deletion of *Mll4* in adult myofibers disturbs the quiescence of MuSCs, TA and soleus muscles were analyzed to quantify Pax7-positive MuSCs. Mll4$^{\Delta HSA}$ mice showed depletion of MuSCs in both muscles (Figure 26A-C). To assess whether the loss of adult quiescent MuSCs in Mll4$^{\Delta HSA}$ mice is associated with their entry into the cell cycle, I quantified Ki67-positive MuSCs in the TA muscles. In Mll4^{WT} TA muscles, there was a negligible presence of Ki67^{+}Pax7^{+} cells, whereas Mll4$^{\Delta HSA}$ muscles showed an increase of Ki67^{+}Pax7^{+} cells (Figure 26D-E). This suggests that ablation of *Mll4* in myofibers at the adult stage causes MuSCs to exit quiescence and enter the cell cycle, leading to the depletion of MuSCs. To examine if adult Mll4$^{\Delta HSA}$ muscle shows an increased number of differentiated MuSCs, I performed an immunocytochemistry assay on sorted MuSCs (Figure 27A-B) to quantify MyoD-positive cells. Compared to the Mll4^{WT} MuSCs, Mll4$^{\Delta HSA}$ MuSCs showed an increased number of MyoD-expressing cells (Figure 28A-B). For detecting MuSCs that entered the cell cycle, I treated EdU for 2 weeks in Mll4$^{\Delta HSA}$ mice (Figure 28C). This long-term EdU labeling method was applied to identify the scarcely dividing MuSCs in adult muscle tissue (Bjornson et al., 2012). I found that the population of MyoD-expressing cells among EdU-positive, dividing MuSCs was also increased in Mll4$^{\Delta HSA}$ muscles (Figure 28D). On the other hand, given that adult quiescent MuSCs can differentiate without entering the cell cycle (Bjornson et al., 2012), I also quantified MyoD-expressing cells among EdU-negative, non-dividing MuSCs. Interestingly, Mll4$^{\Delta HSA}$ MuSCs showed an increased number of MyoD-positive cells among EdU-negative MuSCs (Figure 28E). This

indicates that the deletion of Mll4 in adult muscles causes adult MuSCs to lose their quiescence and undergo differentiation, either with or without dividing.

To test whether the differentiated myogenic progeny of Mll4$^{\Delta HSA}$ muscles fuse into myofibers, I conducted a histological analysis and quantified EdU-positive nuclei located on the inner side of dystrophin structure (Bjornson et al., 2012) (Figure 29A). While the number of fiber-incorporating EdU-positive nuclei was extremely low in control muscles, it was sevenfold higher in Mll4$^{\Delta HSA}$ muscles compared to the control group (Figure 29B). This suggests that *Mll4* deficiency in adult muscles causes MuSCs to exit quiescence and undergo differentiation, with at least some, or perhaps all, of these differentiated cells subsequently fusing into myofibers. This eventually results in severe MuSC loss in adult muscles.

Figure 26. MuSC deprivation in *Mll4* deleted adult myofibers due to increased MuSC activation. (A) Immunohistochemistry on TA muscle section with DAPI (blue), anti-laminin (green), and anti-Pax7 (red). (B) Pax^{+} MuSC number per 100 fibers of $Mll4^{WT}$ and $Mll4^{\Delta HSA}$ TA and (C) soleus muscle. Scale bars, 20 μm. (D) Immunohistochemistry on TA muscle section with DAPI (blue), anti-Ki67 (green), and anti-Pax7 (red). Scale bars, 20 μm. (E) $Pax7^{+}Ki67^{+}$ cell number per total $Pax7^{+}$ cells. (B, C, E) n=3-4 mice for each genotype. Data are presented as mean ± SEM of biological replicates. Statistical analyses were performed using unpaired t-test with Welch's correction.

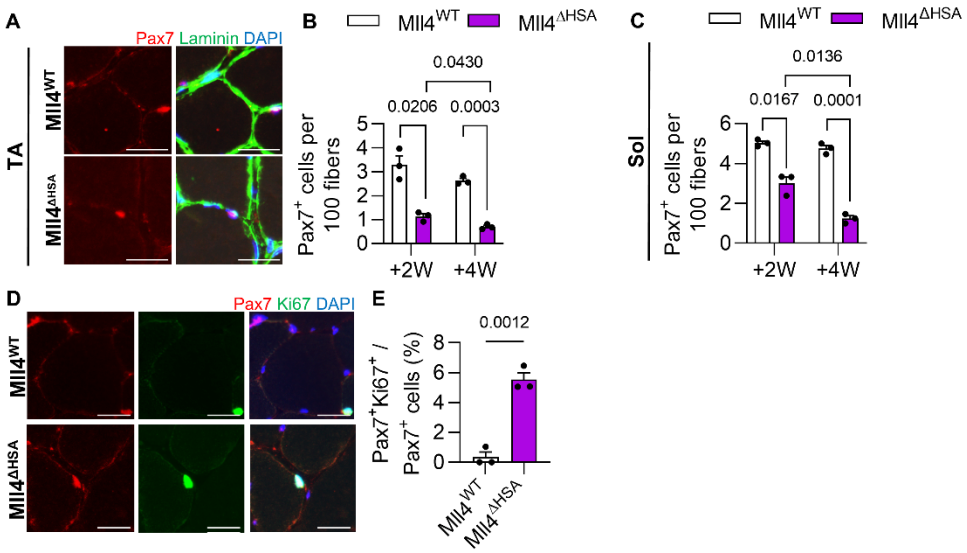
A
Pax7 Laminin DAPI
TA
Mll4WT
Mll4ΔHSA
B
Mll4WT
Mll4ΔHSA
0.0430
0.0206
0.0003
Pax7+ cells per 100 fibers
+2W
+4W
C
Mll4WT
Mll4ΔHSA
0.0136
0.0167
0.0001
Sol
Pax7+ cells per 100 fibers
+2W
+4W
D
Pax7 Ki67 DAPI
Mll4WT
Mll4ΔHSA
E
0.0012
Pax7+Ki67+ / Pax7+ cells (%)
Mll4WT
Mll4ΔHSA

Figure 27. Flow cytometry of cell surface markers of limb muscles to isolate MuSCs. (A-B) Gating strategies for isolating MuSCs in $Mll4^{\Delta HSA}$ muscles with control $Mll4^{WT}$ muscles for each group. Each figure is representative of n = 3 mice. Data are presented as mean ± SEM of biological replicates. Statistical analyses were performed using unpaired t-test with Welch's correction.

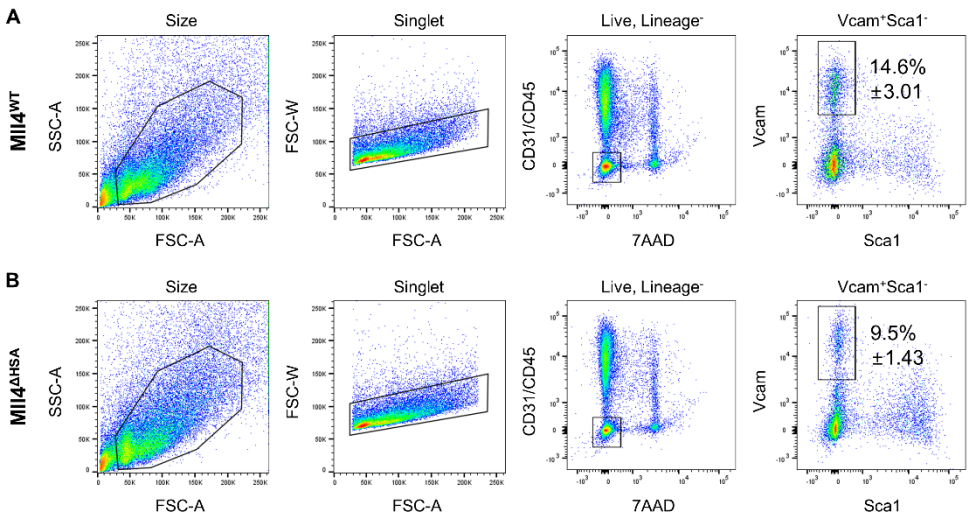
A
Size
Singlet
Live, Lineage-
Vcam+Sca1-
MII4WT
SSC-A
FSC-A
FSC-W
FSC-A
CD31/CD45
7AAD
Vcam
Sca1
14.6%
±3.01
B
Size
Singlet
Live, Lineage-
Vcam+Sca1-
MII4ΔHSA
SSC-A
FSC-A
FSC-W
FSC-A
CD31/CD45
7AAD
Vcam
Sca1
9.5%
±1.43

Figure 28. Aberrant MuSC differentiation in adult Mll4$^{\Delta HSA}$ mice. (A) Immunocytochemistry of sorted MuSCs with DAPI (blue), anti-Pax7 (red), anti-MyoD (green), and EdU (white – pseudo color for Alexa Fluor 647). MyoD^{+} cells and EdU^{+} cells are marked with arrowheads and sharps, respectively. Scale bars, 20 μm. For enlarged images, Scale bars represent 10 μm. (B) MyoD^{+} cell number per total Pax7^{+} cells. (C) Schematic diagram of EdU treatment. (D) MyoD^{+} cell number per EdU^{+}Pax7^{+} cells, and (E) MyoD^{+} cell number per EdU^{-}Pax7^{+} cells were quantified. (B, D, E) n=3-4 mice for each genotype; >200 sorted MuSCs per mouse were quantified. Data are presented as mean ± SEM of biological replicates. Statistical analyses were performed using unpaired t-test with Welch's correction.

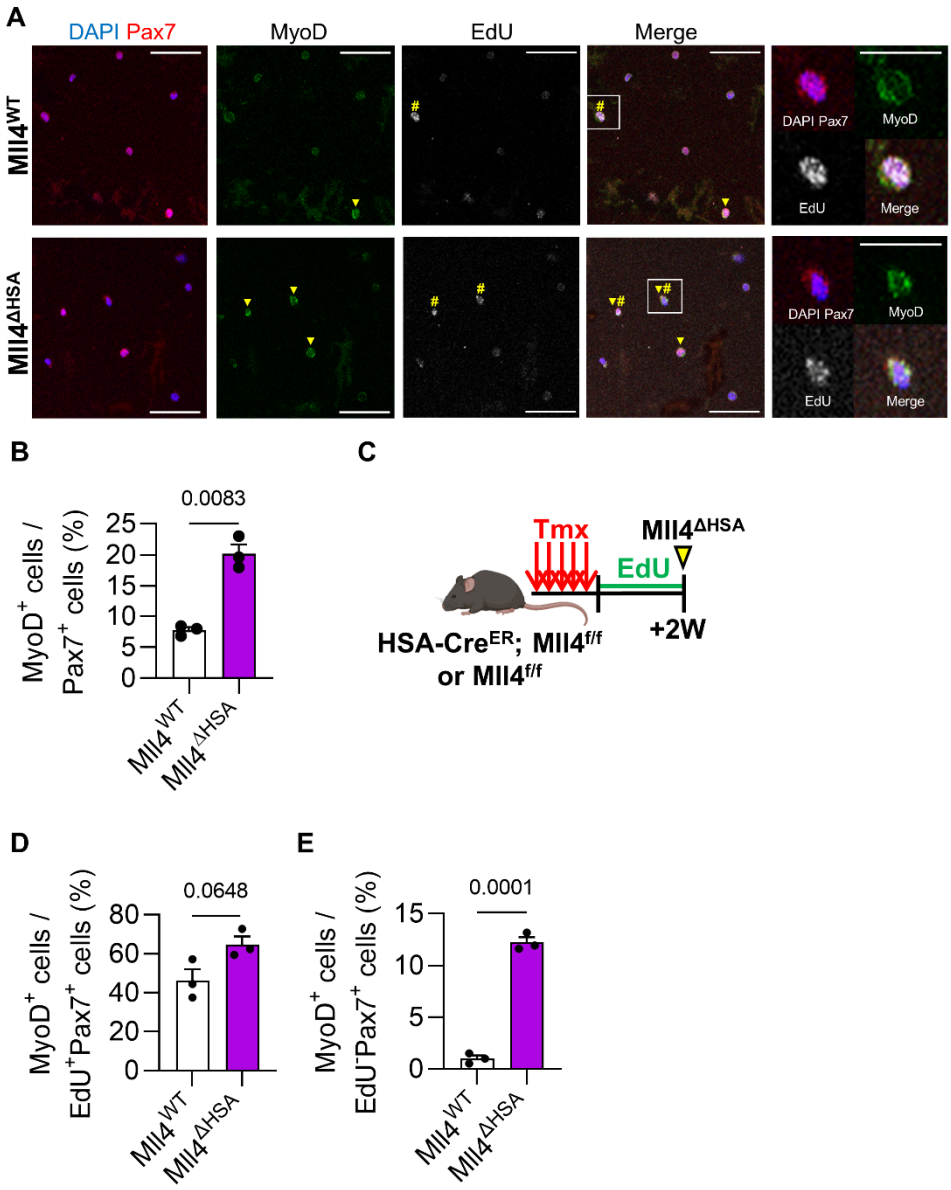
A
DAPI Pax7
MyoD
EdU
Merge
Mll4WT
Mll4ΔHSA
B
0.0083
MyoD+ cells / Pax7+ cells (%)
Mll4WT
Mll4ΔHSA
C
Tmx
EdU
Mll4ΔHSA
+2W
HSA-CreER; Mll4f/f
or Mll4f/f
D
0.0648
MyoD+ cells / EdU+Pax7+ cells (%)
E
0.0001
MyoD+ cells / EdU-Pax7+ cells (%)

Figure 29. Increased fiber fused myoblasts in *Mll4*-deleted myofibers. (A) Immunohistochemistry on TA muscle section with DAPI (blue), EdU (green), and anti-dystrophin (red). Scale bars, 20 μm. For enlarged images, Scale bars represent 10 μm. (B) The number of fiber incorporated EdU^+ cells per 100 fibers. (B) n=3-4 mice for each genotype. Data are presented as mean ± SEM of biological replicates. Statistical analyses were performed using unpaired t-test with Welch's correction.

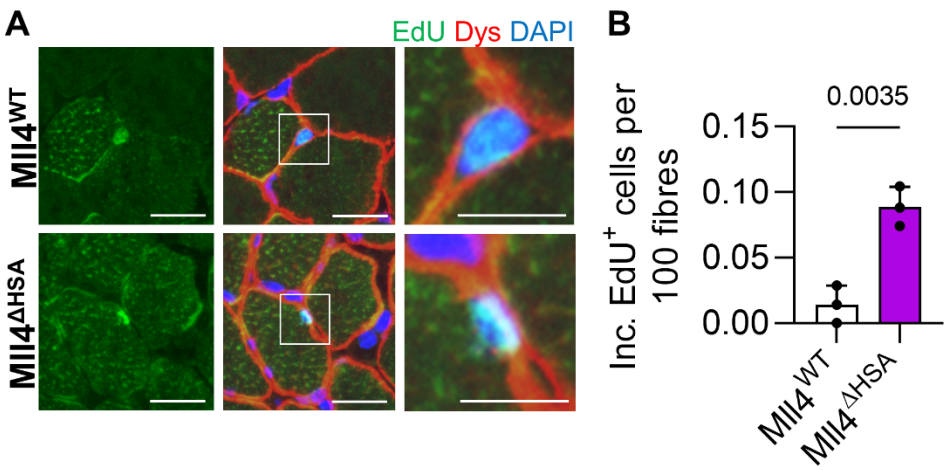
A
EdU Dys DAPI
Mll4WT
Mll4ΔHSA
B
Inc. EdU+ cells per 100 fibres
0.0035
0.15
0.10
0.05
0.00
Mll4WT
Mll4ΔHSA

Lack of *Mll4* impairs muscle regeneration following injury

MuSCs are the primary cell type that contributes to muscle regeneration capacity. To investigate if MuSC depletion in Mll4$^{\Delta HSA}$ mice leads to hindered muscle regeneration, I subjected TA muscles of Mll4^{WT} and Mll4$^{\Delta HSA}$ mice to injury using $BaCl_2$ (hereafter, Mll4$^{WT\text{-}inj}$ and Mll4$^{\Delta HSA\text{-}inj}$) (Figure 30A). Muscles were analyzed 10 days post-injury, as the majority of regenerating fibers are restored (Musarò, 2014). TA muscles of Mll4$^{\Delta HSA\text{-}inj}$ mice showed reduced muscle mass compared to that of Mll4$^{WT\text{-}inj}$ mice, while adjacent muscles such as the EDL, GA, and soleus remained unaffected (Figure 30B). Histological analysis of muscle sections revealed active muscle regeneration in Mll4$^{WT\text{-}inj}$ muscles, as indicated by the predominance of myofibers with centrally located nuclei and relatively homogenous fiber sizes. Conversely, Mll4$^{\Delta HSA\text{-}inj}$ muscle was observed with disorganized tissue architecture with residual damaged fibers that failed to undergo effective regeneration. (Figure 30C). Moreover, Mll4$^{\Delta HSA\text{-}inj}$ mice showed reduced CSA of regenerating fibers (Figure 30D). These results suggest that lack of MuSCs due to the deletion of myofiber-specific Mll4 resulted in severely impinged muscle regeneration capacity.

Figure 30. Defective muscle regeneration capacity after injury in *Mll4* deleted TA muscles. (A) Schematic diagram of muscle injury and mouse preparation. (B) Muscle mass of TA, EDL, GA, and soleus muscles of $Mll4^{WT\text{-}inj}$ and $Mll4^{\Delta HSA\text{-}inj}$ mice. (C) Representative image of TA muscle labeled with anti-laminin (green) and Hoechst 33342. Scale bars, 100 μm. (D) Percentage of myofibers within each indicated range of CSA in TA muscle of $Mll4^{WT\text{-}inj}$ and $Mll4^{\Delta HSA\text{-}inj}$ mice. (B and D) n=3 mice for each genotype. Data are presented as mean ± SEM of biological replicates. Statistical analyses were performed using unpaired t-test with Welch's correction.

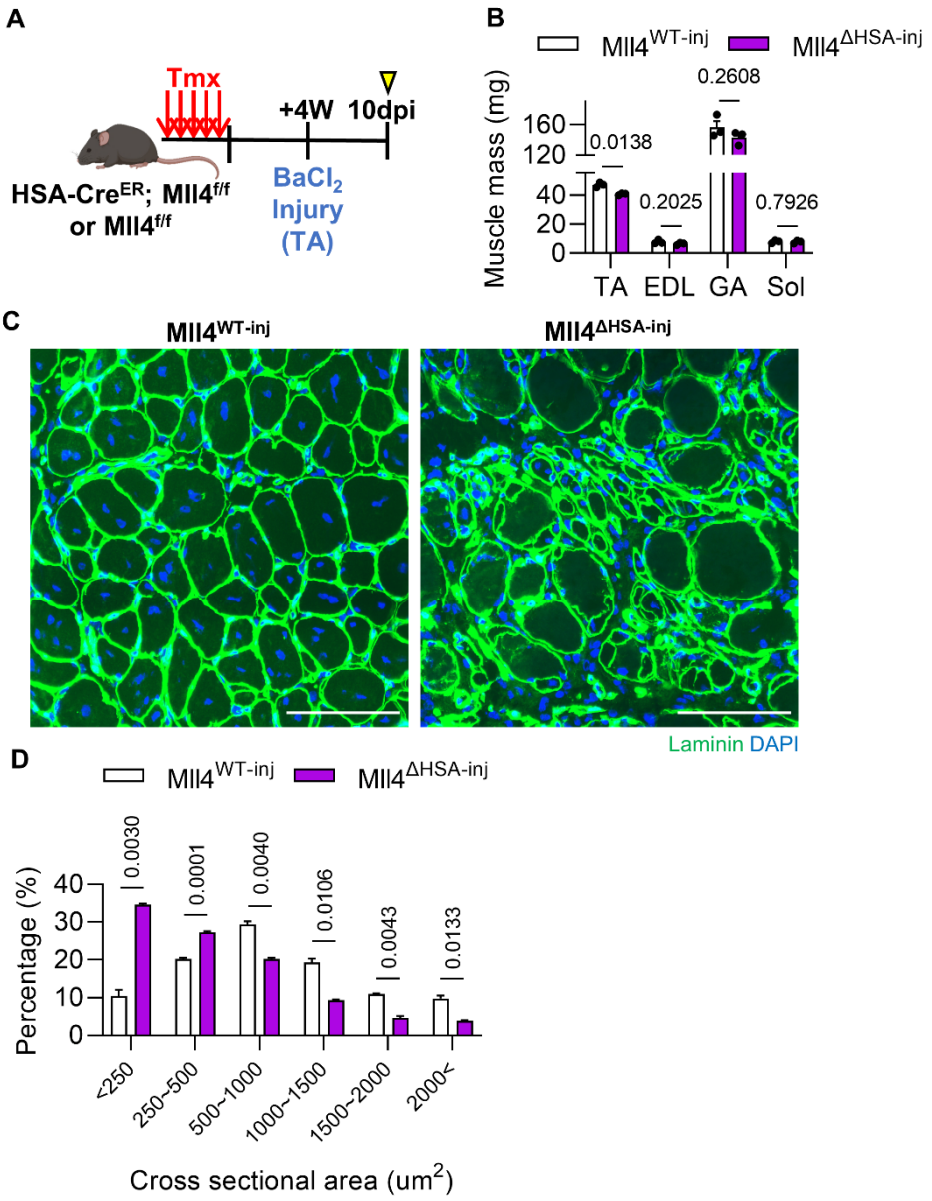
A
Tmx
+4W
10dpi
HSA-Cre^ER; Mll4^f/f
or Mll4^f/f
BaCl2
Injury
(TA)
B
Mll4^WT-inj
Mll4^ΔHSA-inj
Muscle mass (mg)
160
120
40
20
0
0.0138
0.2025
0.2608
0.7926
TA
EDL
GA
Sol
C
Mll4^WT-inj
Mll4^ΔHSA-inj
Laminin DAPI
D
Mll4^WT-inj
Mll4^ΔHSA-inj
Percentage (%)
40
30
20
10
0
0.0030
0.0001
0.0040
0.0106
0.0043
0.0133
<250
250~500
500~1000
1000~1500
1500~2000
2000<
Cross sectional area (um2)

Mll4 in myofibers affects the MuSC niche by regulating Notch ligand expression

To explore how *Mll4* in myofibers may have affected the MuSC niche, I screened for downstream effector candidate genes by analyzing public datasets. For one, I analyzed data curated by Liu et al. (2016) This provided a list of downregulated genes in muscle from MLL4-SET-knockout (KO) mice, where the enzymatic SET domain of MLL4 is ablated, compared to control mice. In addition, I analyzed data from Lee et al. (2013), to obtain the list of downregulated genes in cultured, differentiated Mll4-KO myocytes versus control. Sixty-six genes were identified as commonly downregulated from the two datasets. Since myofiber can directly regulate the MuSC niche via signaling through ligand-receptor interactions (Skelly et al., 2018), I then identified ligands from the 66 candidate genes by comparing them to the mouse ligand database. Consequently, 5 genes were identified as ligand-coding genes that are downregulated by Mll4 KO in both whole muscle and differentiated myocytes. To my surprise, the Notch ligand Jag2 was among the 5 candidate genes. Also, Dll1, another Notch ligand, was identified as downregulated in Mll4 KO myocytes. (Figure 31A).

For MuSCs, Notch signaling is a major signaling pathway that maintains the stem cell pool. When the Notch downstream effector Rbpj is deleted in adult MuSCs, which are predominantly in a quiescent state, they exit the quiescent state and undergo aberrant differentiation (Bjornson et al., 2012; Mourikis et al., 2012). Myofiber-specific deletion of Dll4, a Notch ligand that is mainly expressed in adult myofibers, induces premature differentiation of MuSCs, resulting in a reduced number of stem cells (Eliazer et al., 2022; Kann et al., 2019). These studies suggest

that the maintenance of MuSC quiescence is highly dependent on Notch signaling between MuSCs and myofibers. Considering that the depletion of MuSCs was observed in both Notch signaling-reduced MuSCs and myofiber-specific *Mll4*-deleted (Mll4$^{\Delta MCK}$ and Mll4$^{\Delta HSA}$) MuSCs, I sought to validate the downregulation of Notch ligands in Mll4$^{\Delta MCK}$ and Mll4$^{\Delta HSA}$ mice.

A previous study found that *Dll4* is highly expressed in adult myofibers (Eliazer et al., 2022). In addition, I reported that myofibers of 4-week-old mice exhibited robust expression of *Dll1* and *Jag1* proteins (Kim et al., 2016). Considering that Notch ligands have a fluctuating expression pattern in muscles throughout the developmental stages, I compared mRNA quantity for Notch ligands in the myofibers of wild-type pubertal 4-week-old and adult mice (Figure 32A). Interestingly, genes having dominant expression during each time point correlated with genes that were downregulated due to *Mll4* depletion in muscle fibers. While expression of major Notch ligands of pubertal 4-week-old myofibers – *Jag1* and *Dll1* – decreased in 4-week-old Mll4$^{\Delta MCK}$ myofibers (Figure 32B), the primary Notch ligands of adult myofibers – *Jag2* and *Dll4* – decreased in adult Mll4$^{\Delta HSA}$ myofibers (Figure 32C). In other words, *Mll4* insufficiency in myofibers disturbed Notch ligand expression that is dominant in each pubertal or adult muscle.

To test if Notch signaling is indeed reduced in 4-week-old Mll4$^{\Delta MCK}$ and adult Mll4$^{\Delta HSA}$ MuSCs, the mRNA levels of canonical Notch effectors – *HeyL, Hey1,* and *Hes1* – were quantified via qRT-PCR. As expected, the overall expression of genes

mentioned above was downregulated in both Mll4$^{\Delta MCK}$ and adult Mll4$^{\Delta HSA}$ MuSCs (Figure 32D-E).

Considering the molecular feature of MLL4, I analyzed public ChIP-seq data of MLL4 in myocytes (Lee et al., 2013), to examine whether it may modulate the transcription of Notch ligands on the chromosomal level. This revealed the genomic binding of MLL4 on *Dll1* and *Jag2* gene loci, where *Mll4* deletion reduced H3K4me1 and H3K27ac levels on enhancers for both *Dll1* and *Jag2* genes (Figure 33A-B). This implicates the possibility of MLL4 directly regulating the induction of different Notch ligand gene expressions. Taken together, MLL4 can control diverse Notch ligand expression in myofibers, which is necessary for regulating the MuSC niche during and after postnatal myogenesis.

Figure 31. Evaluation of three public databases. (A) Notch ligands such as Jag2 and Dll1 are downregulated in *Mll4*-deleted muscle and myocyte.

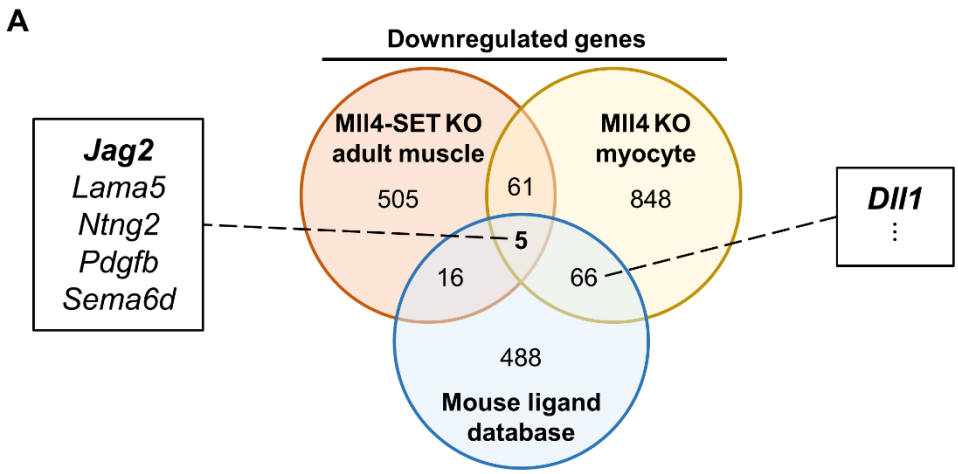
A
Downregulated genes
Jag2
Lama5
Ntng2
Pdgfb
Sema6d
Mll4-SET KO
adult muscle
505
61
Mll4 KO
myocyte
848
5
16
66
488
Mouse ligand
database
Dll1
⋮

Figure 32. Altered Notch ligand expression in *Mll4* deleted myofibers, leading to downregulated notch signaling in MuSCs. (A) qRT-PCR analysis to compare Notch ligand expression in pubertal (4W) and adult myofibers. (B-C) qRT-PCR analysis to quantify mRNA expression of Notch ligands in myofibers of 4-week-old $Mll4^{\Delta MCK}$ mice and adult $Mll4^{\Delta HSA}$ mice. (D-E) qRT-PCR of canonical Notch effectors confirmed general downregulation of Notch signaling in $Mll4^{\Delta MCK}$ and $Mll4^{\Delta HSA}$ MuSCs. (A-E) n=3 mice for each genotype. Data are presented as mean ± SEM of biological replicates. Statistical analyses were performed using unpaired t-test with Welch's correction.

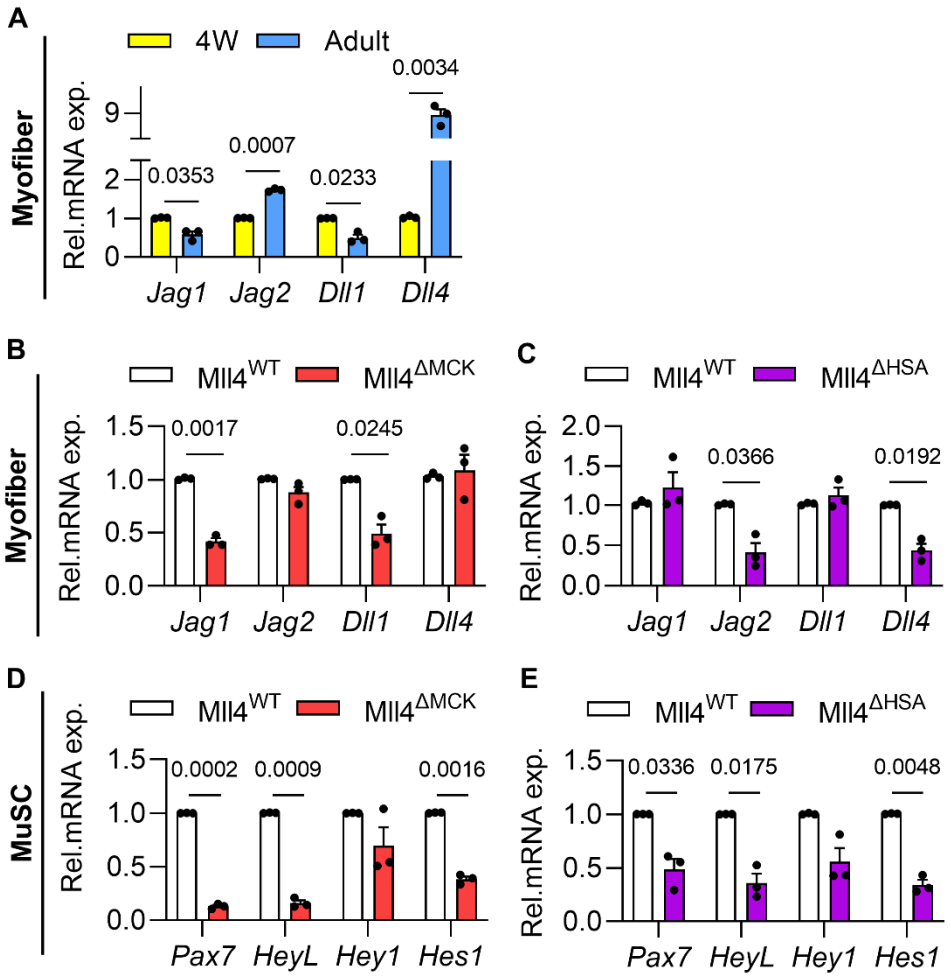
A
Myofiber
4W
Adult
Rel.mRNA exp.
0.0353
0.0007
0.0233
0.0034
Jag1
Jag2
Dll1
Dll4
B
Myofiber
Mll4WT
Mll4ΔMCK
Rel.mRNA exp.
0.0017
0.0245
Jag1
Jag2
Dll1
Dll4
C
Mll4WT
Mll4ΔHSA
Rel.mRNA exp.
0.0366
0.0192
Jag1
Jag2
Dll1
Dll4
D
MuSC
Mll4WT
Mll4ΔMCK
Rel.mRNA exp.
0.0002
0.0009
0.0016
Pax7
HeyL
Hey1
Hes1
E
Mll4WT
Mll4ΔHSA
Rel.mRNA exp.
0.0336
0.0175
0.0048
Pax7
HeyL
Hey1
Hes1

Figure 33. ChIP-seq analysis of MLL4 in myocytes. (A-B) Potential binding site of MLL4 to *Dll1* (A) and *Jag2* (B) gene loci.

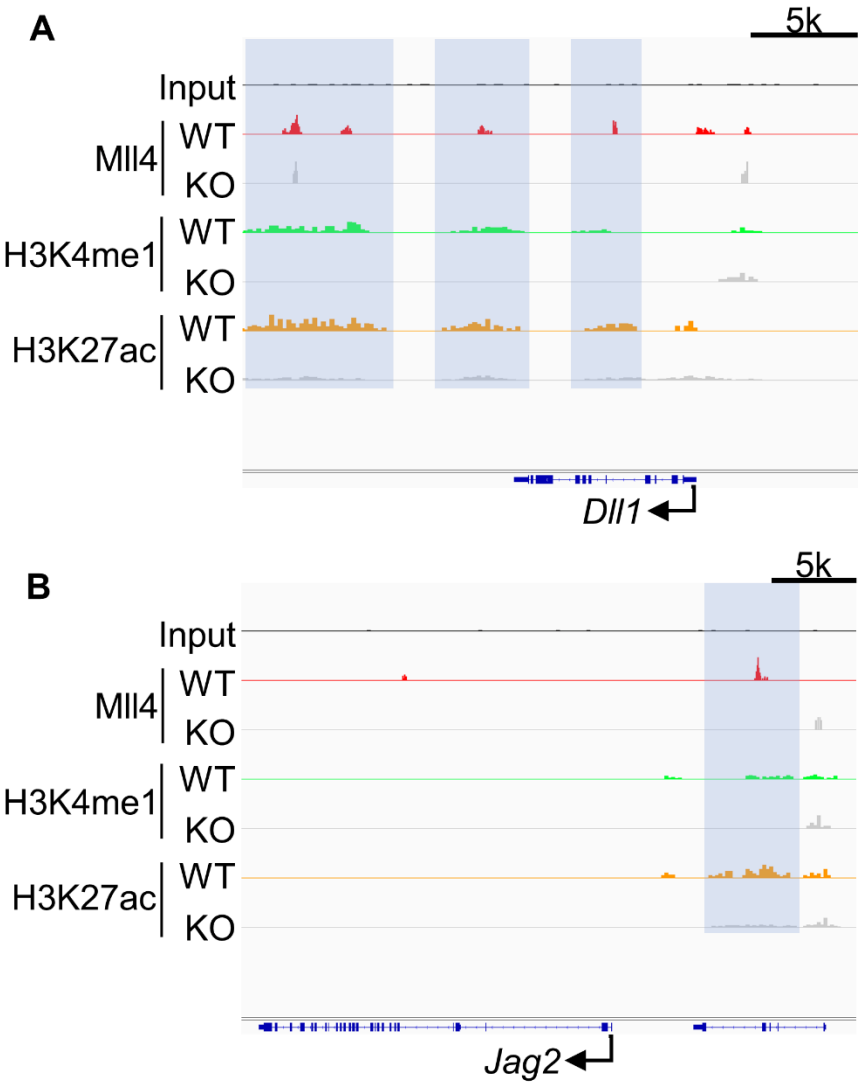
A
5k
Input
Mll4
WT
KO
H3K4me1
WT
KO
H3K27ac
WT
KO
Dll1
B
5k
Input
Mll4
WT
KO
H3K4me1
WT
KO
H3K27ac
WT
KO
Jag2

Discussion

Skeletal muscle has a resilient characteristic due to its resident stem cell populations. Thus, uncovering the mechanism of regulating MuSC fate is crucial for understanding the biological process of developmental and regenerative myogenesis. In this paper, I explored the role of *Mll4* in myofibers regarding the MuSC state regulation and discovered that myofiber-expressed *Mll4* is important for maintaining MuSCs in both muscles during and after postnatal myogenesis. In the pubertal Mll4$^{\Delta MCK}$ muscle, lack of *Mll4* in myofibers resulted in increased population of differentiating myogenic cells, leading to a decrease of MuSCs. Furthermore, induced ablation of *Mll4* in adult myofibers resulted in the quiescence exit of MuSCs, which also caused dramatic depletion of MuSCs. During postnatal myogenesis, juvenile MuSCs constantly proliferate for muscle development (White et al., 2010; Kim et al., 2016). This proliferating cell population decreases due to cell cycle exit during puberty to establish a reserve pool of quiescent MuSCs in adult muscles (Mukund et al., 2020; Frontera and Ochala, 2015). My findings indicate that Mll4 in myofibers are critical for maintaining MuSCs in pubertal muscles, where cycling MuSCs begin to enter quiescence, as well as in adult muscles, where MuSCs remain in a quiescent state. This suggests that *Mll4* plays a critical role in myofibers by creating a microenvironment that supports the maintenance of a healthy population of MuSCs in muscle tissue.

The ability to maintain an adequate number of MuSCs is crucial regardless of gender and age. In this study, I elucidate two critical properties of *Mll4* in preserving the stemness of MuSCs. First, *Mll4* regulates the MuSC number in both sexes. Skeletal muscle exhibits sexual dimorphism in terms of mass, fiber type composition, and contractility attributed to variations in gene expression and hormonal profiles between genders (Haizlip et al., 2015; Takahashi et al., 2024). These differences may have contributed to the disparate muscle phenotypes after the deletion of myofiber-*Mll4* in male and female mice. However, gender did not influence the extent of MuSC depletion resulting from *Mll4* ablation. Secondly, Mll4 regulates MuSC quiescence across different developmental stages, including both during and after postnatal myogenesis. Previous research indicated that myofiber-specific deletion of *Mll4* led to a slow-to-fast fiber type shift (Liu et al., 2020). However, my findings reveal that this phenotype is not present following *Mll4* deletion in adult muscle tissue. The expression of genes related to both slow and fast muscle fibers demonstrated a broad reduction following the deletion of *Mll4*. However, since the altered expression profile was not biased toward a specific fiber type, it did not result in significant physiological changes. Therefore, I suggest that the myofiber phenotype is unlikely to undergo substantial alterations even after prolonged periods post-*Mll4* deletion. This indicates that Mll4 may play a role in the development of myofibers, but not in their maintenance during adulthood, at which developmental myogenesis is complete. Indeed, it is reported that during developmental myogenesis, Foxo/Notch signaling regulates fiber type specification, leading to a reduction in slow fibers and an increase in fast fibers when disrupted in muscle (Kitamura et al., 2007). Considering that (1) this phenotype is in line with that of *Mll4*-mKO mice, as reported previously, and (2) Mll4 has the possibility of regulating the gene

expression of Notch ligands, the deletion of *Mll4* might have disrupted Notch signaling in developing myofibers, leading to aberrant fiber type specification. Altogether, my data provide new insights into the role of Mll4 as a crucial regulator of the MuSC quiescence, highlighting its significance across developmental stages and irrespective of gender (Figure 34A).

Figure 34. Summary figure of the role of Mll4 in myofiber during different developmental stages. (A) During myofiber development, Mll4 prevents the conversion of slow-twitch to fast-twitch myofibers, particularly in male muscles. However, during puberty, Mll4 sustains MuSC populations in both males and females through its regulation of Jag1 and Dll1. In adulthood, Mll4 continues to support the maintenance of MuSCs by modulating Jag2 and Dll4.

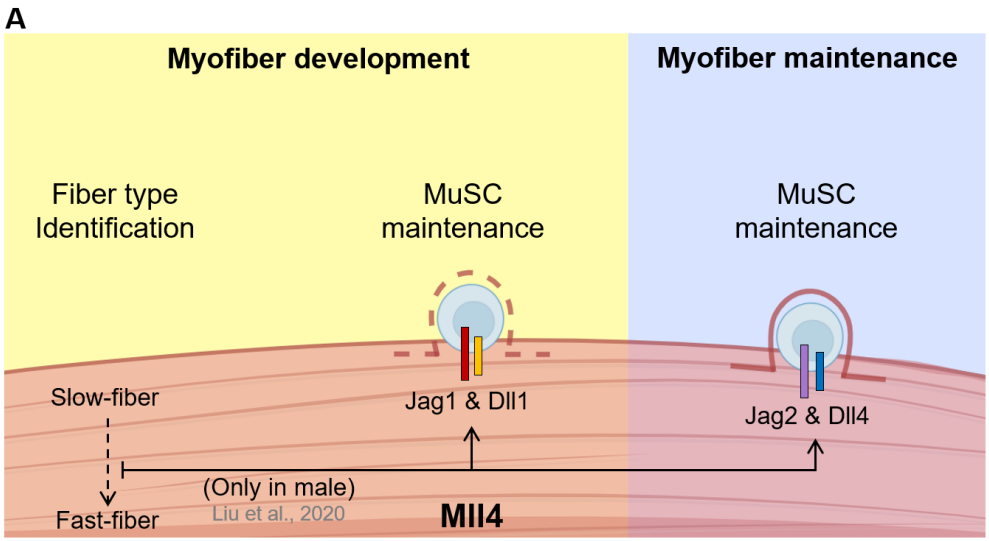
A
Myofiber development
Myofiber maintenance
Fiber type Identification
MuSC maintenance
MuSC maintenance
Slow-fiber
Fast-fiber
Jag1 & Dll1
Jag2 & Dll4
(Only in male)
Liu et al., 2020
Mll4

Chromatin modification of enhancers within myofibers can modulate the expression of extracellular matrix (ECM) components or growth factors, thereby indirectly influencing the MuSC niche (Zhou et al., 2019; Lazure et al., 2020). My study suggests that MLL4, an enhancer activator, regulates Notch ligand expression in myofibers to directly control MuSC quiescence. By analyzing and validating transcriptome databases from previous studies, I verified that the expression of Notch ligands was downregulated in Mll4-KO myocyte. Moreover, an analysis of ChIP-seq data revealed genomic binding of MLL4 on Notch ligand gene loci. The downregulation of Notch ligands in myofibers led to a reduced expression of canonical Notch target genes in MuSCs. This indicates that MLL4 can regulate the signaling pathway that affects adjacent cells. This finding is particularly intriguing given that MLL4 has primarily been studied as a critical factor for activating intracellular signaling pathways, including those related to cancer and cell fate determination (Lee et al., 2013; Wang et al., 2016; Rao et al., 2015; Dhar et al., 2018; Ang et al., 2016). Specifically, in myofibers, Mll4 was reported to activate the transcription of slow-twitch genes (Liu et al., 2020). By inspecting the physiological impact of *Mll4* deletion in myofibers on MuSCs, I revealed that *Mll4* regulates not only intracellular signaling pathways, as previously reported, but also signaling pathways that affect adjacent cells, by controlling expressions of ligand genes. This underscores the importance of exploring the potential gene-regulating activity of MLL4, which may impact other cellular processes, such as differentiation and tumorigenesis, in neighboring cells.

It has been well-established that Notch signaling is a fundamental pathway regulating the MuSC niche in prenatal and postnatal muscles to maintain an appropriate stem cell pool (Siebel et al., 2017; Gioftsidi et al., 2022). In this study, I observed that the phenotype of the myofiber-specific Mll4-cKO was very similar to that of MuSCs with disrupted Notch signaling. MuSCs in both myofiber-specific Mll4-cKO mice and MuSC-specific Notch-cKO mice exhibit reduced expression of canonical Notch target genes (Mourikis et al., 2012; Fujimaki et al., 2018), accompanied by increased expression of MyoD and Ki67 (Mourikis et al., 2012; Fujimaki et al., 2018; Fukada et al., 2011; Noguchi et al., 2019). These changes led to a reduction in MuSC numbers during postnatal muscle development (Fukada et al., 2011) and increased fusion of myoblasts with myofibers in adult muscles, which also resulted in a remarkable loss of MuSCs (Bjornson et al., 2012). These findings support the hypothesis that myofiber-expressed Mll4 may regulate the expression of Notch ligands, thereby modulating Notch signaling in MuSCs and influencing their cell fate.

Previous studies reported that the myofiber is an important source of Notch ligands, sending signals to MuSCs to control their niche and hence their cell fate (Kim et al., 2016; Jo et al., 2022., Fujimaki et al., 2018). Notch ligands have distinct expression patterns in myofibers during development, affecting the MuSC niche in different ways. In this study, I investigated the Notch ligands with prevailing expression in different stages; *Jag1* and *Dll1* in pubertal myofibers, and *Jag2* and *Dll4* in adult muscle fibers. Interestingly, *Mll4* deletion in pubertal and adult myofibers disturbed the expression of Notch ligands that were principally expressed

in each stage. Previously, Eliazer and colleagues reported that myofiber-specific deletion of Dll4 resulted in a reduction of MuSCs. However, the decrease in MuSCs was more pronounced when the pan-Notch regulator Mib1 was deleted from myofibers (Eliazer et al., 2022). This implies the presence of a complementary Notch ligand acting as a signaling factor to maintain MuSC quiescence in adult muscles, together with Dll4. My findings suggest that along with the well-known factor Dll4, Jag2 may be another Notch ligand in adult myofibers contributing to maintaining the $Pax7^{+}$ quiescent stem cells, both of which were found to be regulated by Mll4. Taken together, this study suggests that MLL4 functions as a regulator that modulates the expression of various Notch ligands in myofibers during both pubertal and adult stages. This regulation is essential for the precise control of MuSC quiescence throughout developmental stages.

Mll4 deletion notably hindered H3K4me1 and H3K27ac levels on enhancers for both the *Dll1* gene in pubertal fibers and the *Jag2* gene in adult fibers, indicating different gene regulation of MLL4 in the two developmental stages. This may be attributed to the distinct pioneer transcription factors that recruit MLL4 to induce Notch ligand expression at different developmental stages. Several transcription factors – such as CCAAT/enhancer-binding protein family, myocyte enhancer factor 2 family, and Nrf1 – are identified to bind the DNA to recruit the MLL4 complex (Lee et al., 2013; Wang et al., 2016; Liu et al., 2020; Huisman et al., 2021). Depending on the cell type and differentiation stage, different transcription factors recruit MLL4 to regulate the expression of various genes. Transcription factors associated with Notch signaling have also been identified. A study on chicken

embryos found that a transcription coregulator, Yap, binds to the enhancer of *Jag2* (Esteves et al., 2016). In mice, Notch1 ICD can act as a transcription activator in muscle fibers to activate the gene expression of *Jag2* and *Dll4* (Bi et al., 2016). Following these studies, it is plausible that Yap and Notch ICD may recruit MLL4 to regulate the expression of different Notch ligands in myofibers. Further investigation is required to elucidate the molecular mechanism by which MLL4 regulates Notch ligand gene expression in myofibers. This includes identifying the specific pioneer transcription factors that interact with MLL4 across different developmental stages.

Conclusions

This study suggests a unique function of Mll4 in myofibers controlling MuSC state, possibly by orchestrating different Notch ligand expressions in various developmental stages. Interestingly, this regulatory role of Mll4 appears to be developmentally dynamic, ensuring proper MuSC maintenance during crucial transitions such as puberty and into adulthood. The differential expression of Notch ligands may indicate that Mll4 functions as a molecular switch, adapting to the specific needs of muscle stem cells at various life stages.

Moreover, despite skeletal muscle being known to exhibit sexual dimorphism, the role of Mll4 regulating MuSCs was valid in both male and female mice, highlighting its conserved function across sexes. This finding underscores the universality of Mll4's role in muscle biology and raises intriguing questions about its molecular mechanisms of regulating gene transcription of Notch ligands in muscle tissue. By elucidating an additional mechanism governing MuSC maintenance, this research opens new avenues for the biological manipulation of muscle stem cells, potentially paving the way for novel therapeutic strategies in muscle regeneration and repair.

Materials and Methods

Animals

MCK$^{Cre/+}$ (stock 006475), *HSA*$^{MerCreMer/+}$ (stock 031934), and *Mll4*$^{f/f}$ (stock 032152) mice were acquired from The Jackson Laboratory (Bar Harbor, ME, USA). The mice were backcrossed to C57BL/6 mice at least 6 times. To generate mice with myofiber-specific deletion of *Mll4*, *Mll4*$^{f/f}$ mice were crossed with *MCK*$^{Cre/+}$ (*MCK*$^{Cre/+}$*; Mll4*$^{f/f}$ *– Mll4*$^{\Delta MCK}$ –). To develop myofiber-specific *Mll4* conditional knockout mice using tamoxifen-inducible Cre, *Mll4*$^{f/f}$ mice were crossed with *HSA*$^{MerCreMer/+}$ (*HSA*$^{MerCreMer/+}$*; Mll4*$^{f/f}$ *– Mll4*$^{\Delta HSA}$ –). Following a breeding strategy from The Jackson Laboratory (Bar Harbor, ME, USA), I bred heterozygous *Mll4*$^{f/+}$ females with Cre-recombinase to homozygous *Mll4*$^{f/f}$ males. Both male and female mice were used in the experiments. Mll4$^{\Delta HSA}$ mice used for experiments were adults, between 3-6 months of age. Control littermates lacking Cre-recombinase (Mll4^{WT}) were utilized for analysis. All mouse lines were housed under controlled conditions that were specific pathogen-free and handled according to the guidelines of the Seoul National University Institutional Animal Care and Use Committee (Protocol number: SNU-240103-3).

Animal procedures

Tamoxifen (Sigma-Aldrich) was dissolved in corn oil at a concentration of 20mg/ml.

For tamoxifen-induced Cre recombination in Mll4$^{\Delta HSA}$ mice, both control and experimental mice were administered tamoxifen at a concentration of 150 mg/kg of mouse per day for five continuous days by intraperitoneal injection. For detection of cell cycle entry, 5-ethynyl-2'-deoxyuridine (EdU; Thermo Fisher Scientific) dissolved in sterile phosphate-buffered saline (PBS) was injected at a concentration of 40 mg/kg of mouse intraperitoneally daily.

Muscle injury

For $BaCl_2$ muscle injury, mice were anesthetized with 2.4% 2, 2, 2-Tribromoethanol (Avertin; Sigma-Aldrich) in PBS (240 mg/kg of mouse) and injected with 50 µl 1.2% $BaCl_2$ in saline (Sigma-Aldrich) to the tibialis anterior (TA) muscles. At 10 days after the injury, TA muscles were dissected, frozen in optimal cutting temperature compound (O.C.T.; Sakura Finetek) with liquid nitrogen, and stored at -80°C until analysis.

Measurement of CSA distribution

Laminin-stained section was imaged with EVOS FL Auto 2 (Thermo Fisher Scientific) with the same laser setting, exposure, and magnification. To measure CSA, semiautomatic muscle analysis using segmentation of histology (SMASH) was used with a segmentation filter (CSA between 200 µm2 and 6000 µm2; eccentricity ≤0.95; convexity ≥0.80). For injured muscles, CSA of regenerating myofibers with centralized nuclei was analyzed. The segmentation filter was adjusted as follows: CSA between 150 µm2 and 6000 µm2; eccentricity ≤0.95; convexity ≥0.80.

Single myofiber isolation

Single myofiber isolation was performed according to a previously reported protocol with modifications (Gallot et al., 2016). Dissected hindlimb extensor digitorum longus (EDL) muscles were enzymatically digested in Dulbecco's modified Eagle's medium (DMEM; Hyclone) containing 2.5% HEPES (Sigma-Aldrich) and collagenase II (800 units/mL, Worthington) at 37℃ for 60 min. Digested muscles were blocked in Dulbecco's modified Eagle's medium and 10% horse serum (Hyclone). The single myofibers were released by gentle trituration. Undamaged and noncontracted single myofibers were then washed with PBS several times and collected for immunocytochemistry and RNA extraction. This protocol yields a single myofiber with MuSCs attached. Consequently, RNA extracted from isolated myofibers may include a minimal fraction of MuSC-derived RNA.

Muscle stem cell (MuSC) isolation

Isolation of MuSC was performed according to a previously reported protocol with modifications (Liu et al., 2015). Limb muscles were dissected and mechanically dissociated in DMEM containing 10% horse serum, collagenase II (800 units/mL), and dispase (1.1 units/mL, Thermo Fisher Scientific) at 37℃ for 40 min. Digested suspensions were subsequently triturated by sterilized syringes with 20G 1/2 needle (BD Biosciences) and washed with DMEM to harvest mononuclear cells. Mononuclear cells were stained with anti-Sca-1-Pacific blue (Biolegend), anti-CD31-APC (Biolegend), anti-CD45–APC (Biolegend), and anti-Vcam1-Biotin (BD

Biosciences). PE-Cy7- Streptavidin (Biolegend) was used as a secondary reagent. To exclude dead cells, 7-AAD (Sigma-Aldrich) was used. Stained cells were analyzed and $Vcam1^{+}Sca1^{-}$ 7-$AAD^{-}CD31^{-}$ $CD45^{-}$ MuSCs were isolated using FACS Aria III cell sorter (BD Biosciences) with 4-way-purity precision. FACS gating strategy was referred to the previously reported protocol (Liu et al., 2015). Isotype control density plots were used as a reference for positive gating. Freshly isolated MuSCs were attached to a slide glass by cytospin for immunocytochemistry, or collected for RNA and protein extraction.

Immunohistochemistry

Freshly dissected TA or Soleus muscles were embedded in O.C.T., snap-frozen in liquid nitrogen, and stored at -80°C prior to sectioning. Cross-sectional 7 μm-thick sections were obtained from the embedded muscles using a cryostat. For myosin heavy chain (MyHC) staining, unfixed muscle sections were incubated overnight at 4 °C with mouse anti-MyHC type 1 (DSHB, BA-D5, 1:10) or mouse anti-MyHC type 2x (DSHB, 6H-1, 1:5) in addition to rat anti-laminin (Abcam, ab11576, 1:1000 dilution) in 3% BSA blocking buffer. After washes in PBS, sections were incubated for 1 h with 1:500 dilution of Alexa Fluor 488-goat anti-mouse MIgG2b (Invitrogen), or Alexa Fluor 488-conjugated anti-mouse IgM (Invitrogen), and Alexa Fluor 594-conjugated anti-rat IgG (Invitrogen). For staining myoblasts, sections were fixed in 4% paraformaldehyde (PFA) for 10 min, and washed in PBS. Antigen retrieval was then performed in citrate buffer (10 mM citric acid, pH 6) at 95°C 15 min. The sections were blocked by mouse Ig blocking reagent and blocking buffer from M.O.M. Kit (Vector Laboratories), according to the manufacturer's protocol. Then,

the sections were incubated with primary antibodies in the blocking buffer at 4 °C overnight. The primary antibodies used include mouse anti-Pax7 (1:100, DSHB), rabbit anti-Ki67 (1:500, Sigma-Aldrich), mouse anti-MyoG (1:100, DSHB), rabbit anti-Dystrophin (1:500, Abcam), rabbit anti-Laminin (1:500, Sigma-Aldrich), and rabbit anti-cleaved Caspase-3 (1:200, Cell Signaling Technologies). After washing the sections with PBS, the sections were stained with secondary antibodies for 1 hr at RT, washed, and mounted. The secondary antibodies were used at a concentration of 1:400 and include goat anti-Rabbit IgG-Alexa Fluor 488 (Thermo Fisher Scientific), goat anti-Rabbit IgG-Alexa Fluor 594 (Thermo Fisher Scientific), and goat anti-Mouse IgG-Alexa Fluor 594 (Thermo Fisher Scientific). Hoechst 33342 (1:2,000, Thermo Fisher Scientific) was used to visualize nuclei. For EdU staining, I used the Click-iT EdU Alexa Fluor 488 Imaging Kit (Thermo Fisher Scientific) following the manufacturer's protocol before the blocking step. The number of each cell type and myofibers was counted in the total TA or Soleus area, and representative images were selected in the same region of the section used in the cell counting. Imaging was conducted with EVOS FL Auto 2 (Thermo Fisher Scientific).

Immunocytochemistry

For isolated myofibers staining, freshly isolated myofibers were fixed immediately following FACS isolation. The total time required to fix freshly isolated MuSCs after enzymatic dissociation was less than 3 hours. Fixation was done using 4% PFA for 10 min at room temperature (RT), quenched in 0.1M glycine in PBS for 10 min at RT, and blocked for 1 hour at RT by blocking buffer (5% goat serum and 5% bovine serum albumin in PBS/0.4% Triton X-100). Then, the myofibers were incubated

with mouse anti-Pax7 (1:100, DSHB) in the blocking buffer at 4 °C overnight. After washing the myofibers three times with PBS/0.1% Triton X-100, the myofibers were stained with goat anti-Mouse IgG-Alexa Fluor 594 (1:400, Thermo Fisher Scientific) and Hoechst 33342 (1:5,000, Thermo Fisher Scientific) for 1 hour at RT, washed and mounted on slide glass. Imaging was conducted with EVOS FL Auto 2 (Thermo Fisher Scientific). For isolated MuSCs staining, freshly isolated MuSCs were attached to a slide glass by cytospin and fixed by 4% PFA for 10 min at RT. The fixed MuSCs were washed with PBS/0.4% Triton X-100 several times and blocked with blocking buffer (5% goat serum and 5% bovine serum albumin in PBS/0.4% Triton X-100) for 1 hour at RT and incubated with mouse anti-Pax7 (1:100, DSHB) and rabbit anti-MyoD (1:200, Santa Cruz) overnight at 4°C. The slides were washed with PBS/0.1% Triton X-100 several times and incubated with goat anti-Mouse IgG-Alexa Fluor 594 (1:400, Thermo Fisher Scientific) and goat anti-Rabbit IgG-Alexa Fluor 488 (1:400, Thermo Fisher Scientific). For EdU staining, I used the Click-iT EdU Alexa Fluor 647 Imaging Kit (Thermo Fisher Scientific) following the manufacturer's protocol before the blocking step. The slides were counterstained with Hoechst 33342 (Thermo Fisher Scientific) and mounted. Imaging was conducted with EVOS FL Auto 2 (Thermo Fisher Scientific).

Four limb grip strength measurement

Grip strength was assessed by using a grip strength test meter (grip strength test BIO-GS3, Bioseb). Mice were allowed to grasp a grid attached to the tester with 4 limbs and were manually pulled in a horizontal direction by the tip of the tail. The test was performed 5 times with 10 min of resting between each measurement. The average

of the top 3 result value (N, Newton) was normalized to body weight (g) (N/g). All experiments were performed in a blinded fashion.

Chronic exercise training and endurance running test

Randomized mice were pre-acclimated to the treadmill (DJ2-242, Dual Treadmill, Daejeon, Korea) before training. The scheme consists of exploration (0m/min for 5 min), and subsequent running (5m/min for 5 min, 10m/min for 5 min, 15m/min for 5 min). After 3 days of acclimation, mice were subjected to chronic exercise training for 5 weeks, 5 days per week with a protocol of 5m/min for 5min, 10m/min for 5min, 15m/min for 30 min. To test endurance running capacity, mice were allowed to run until exhaustion with speed set to 10m/min for 30 min and incremented by 2m/min every 20 min with no inclination. Exhaustion was defined as the condition where mice remained stationary at the end of the treadmill for more than 10 seconds despite mechanical stimulation. All experiments were performed in a blinded fashion.

RNA extraction and quantitative real-time polymerase chain (qRT-PCR)

Total RNA was extracted from freshly isolated myofibers (100 myofibers per mouse) and MuSCs (5,000-10,000 cells per mouse) using a TRIzol Reagent (Life Technologies) and analyzed by qRT-PCR. First-strand complementary DNA was synthesized from 1 μg of RNA using ReverTra Ace (Toyobo) containing random oligomer according to the manufacturer's instructions. qRT-PCR (Qiagen) was performed with SYBR Green technology (SYBR Premix Ex Taq, Qiagen) using specific primers against indicated genes. Relative mRNA levels were determined

using the $2^{-\Delta\Delta Ct}$ method and normalized to *Gapdh*. Primers are listed in Supplementary Table 1.

Table 1. Primers used for RT-qPCR analysis.

Gene	Forward (5'-3')	Reverse (5'-3')
Gapdh	TCATGACCACAGTCCATGCC	CAGATCCACGACGGACACAT
Mll4	GCTATCACCCGTACTGTGTCAACA	CACACACGATACACTCCACACAA
Dll1	TGGGGCTACCCAGATCAAGA	CAGGAATCTCCCCACCCCTA
Dll4	GGAACCTTCTCACTCAACATCC	CTCGTCTGTTCGCCAAATCT
Jag1	CCTCGGGTCAGTTTGAGCTG	CCTTGAGGCACACTTTGAAGTA
Jag2	CAATGACACCACTCCAGATGAG	GGCCAAAGAAGTCGTTGCG
Pax7	CGATTAGCCGAGTGCTCAG	GGAGGTCGGGTTCTGATTCC
Hes1	CCAGCCAGTGTCAACACGA	AATGCCGGGAGCTATCTTTCT
Hey1	TCAGAGCAGTGAGGTGAAGG	AGTGCAGGCAAGTCTACAT
Heyl	GCTCGTATGTCTGGTGCTGA	CACTCCCTGAAGACGAAAGC
Myh7	CTCAAGCTGCTCAGCAATCTATTT	GGAGCGCAAGTTTGTCATAAGT
Tnni1	TGAAGCCAAATGCCTCCACAACAC	ACACCTTGTGCTTAGAGCCCAGTA
Tnnt1	TGGATCCACCAGCTGGAATCAGAA	GCTGATGCGGTTGTAGAGCACATT
Myh4	CACCTGGACGATGCTCTCAGA	GCTCTTGCTCGGCCACTCT
Tnni2	AGCAGCAAGGAGCTGGAAGA	ATGGCGTCGGCAGACATAC
Tnnt3	AACTGGAGACTGACAAATTCGAGT	GCTGTGCTTCTGGGTTTGGT
Tnnc2	CCATCATCGAGGAGGTGGAC	CTTCCCCTTCGCATCCTCTT
Ldhb	AGTCTCCCGTGCATCCTCAA	AGGGTGTCCGCACTCTTCCT
Ppp1r1a	CACCTGGGATCCCAGACACA	GGGGTTGGATTCTGCAGACT
Phyhd1	CTCTGCATGCCCATGACCC	CTTCGCCGCCAAAGTGAG
Dgat2	GCTGGTGCCCTACTCCAAG	CCAGCTTGGGGACAGTGA
Fads6	GGTAGCTCTTGAGCATTTGAGG	AGTAAAGGCCCAGGCAGATG
Cpt1b	GAGTGACTGGTGGGAAGAATATG	GCTGCTTGCACATTTGTGTT

Statistical analysis

Sample size determination was based on anticipated variability and effect size that was observed in the investigator's lab for similar experiments. For quantification, individuals performing the counts were blinded to sample identity and randomized. All statistical analyses were performed using GraphPad Prism 9 (GraphPad Software). For comparison of significant differences in multiple groups for normally distributed data, statistical analysis was performed by one-way or two-way ANOVA followed by Tukey's pairwise comparison post hoc test. For non-normally distributed data, Brown–Forsythe and Welch ANOVA followed by the Games-Howell multiple comparisons test was used. For the comparison of the two groups, Student's unpaired t-test assuming a two-tailed distribution with Welch's correction was used. Unless otherwise noted, all error bars represent s.e.m. The number of biological replicates and statistical analyses for each experiment were indicated in the figure legends. Independent experiments were performed at least in triplicates.

References

Frontera, W.R., and Ochala, J. (2015). Skeletal muscle: a brief review of structure and function. *Calcif. Tissue Int.* **96**, 183–195.

Witzemann, V. (2006). Development of the neuromuscular junction. *Cell Tissue Res.* **326**, 263–271.

Tajbakhsh, S. (2009). Skeletal muscle stem cells in developmental versus regenerative myogenesis. *J. Intern. Med.* **266**, 372–389.

Kang, J.S., and Krauss, R.S. (2010). Muscle stem cells in developmental and regenerative myogenesis. *Curr. Opin. Clin. Nutr. Metab. Care* **13**, 243–248.

Hernandez-Hernandez, J.M., Garcia-Gonzalez, E.G., Brun, C.E., and Rudnicki, M.A. (2017). The myogenic regulatory factors, determinants of muscle development, cell identity and regeneration. *Semin. Cell Dev. Biol.* **72**, 10–18.

Kim, J.H., Han, G.C., Seo, J.Y., Park, I., Park, W., Jeong, H.W., Lee, S.H., Bae, S.H., Seong, J., Yum, M.K., et al. (2016). Sex hormones establish a reserve pool of adult muscle stem cells. *Nat. Cell Biol.* **18**, 930–940.

Best, T.M., and Hunter, K.D. (2000). Muscle injury and repair. *Phys. Med. Rehabil. Clin. N. Am.* **11**, 251–266.

Eliazer, S., Sun, X., Barruet, E., and Brack, A.S. (2022). Heterogeneous levels of delta-like 4 within a multinucleated niche cell maintain muscle stem cell diversity. *eLife* **11**, e72894.

Eliazer, S., Muncie, J.M., Christensen, J., Sun, X., D'Urso, R.S., Weaver, V.M., and Brack, A.S. (2019). Wnt4 from the niche controls the mechano-properties and quiescent state of muscle stem cells. *Cell Stem Cell* **25**, 654–665.e4.

Farup, J., Madaro, L., Puri, P., and others. (2015). Interactions between muscle stem cells, mesenchymal-derived cells, and immune cells in muscle homeostasis, regeneration, and disease. *Cell Death Dis.* **6**, e1830.

Egan, B., and Zierath, J.R. (2013). Exercise metabolism and the molecular regulation of skeletal muscle adaptation. *Cell Metab.* **17**, 162–184.

Schiaffino, S., and Reggiani, C. (2011). Fiber types in mammalian skeletal muscles. *Physiol. Rev.* **91**, 1447–1531.

Burke, A.C., and Nowicki, J.L. (2003). A new view of patterning domains in the vertebrate mesoderm. *Dev. Cell* **4**, 159–165.

Nassari, S., Duprez, D., and Fournier-Thibault, C. (2017). Non-myogenic contribution to muscle development and homeostasis: The role of connective tissues. *Front. Cell Dev. Biol.* **5**, 22.

Lee, J.E., Wang, C., Xu, S., Cho, Y.W., Wang, L., Feng, X., Baldridge, A., Sartorelli, V., Zhuang, L., Peng, W., and Ge, K. (2013). H3K4 mono- and di-

methyltransferase MLL4 is required for enhancer activation during cell differentiation. *eLife* **2**, e01503.

Wang, C., Lee, J.E., Lai, B., Macfarlan, T.S., Xu, S., Zhuang, L., Liu, C., Peng, W., and Ge, K. (2016). Enhancer priming by H3K4 methyltransferase MLL4 controls cell fate transition. *Proc. Natl. Acad. Sci. USA* **113**, 11871–11876.

Wang, S.P., Tang, Z., Chen, C.W., Shimada, M., Koche, R.P., Wang, L.H., Nakadai, T., Chramiec, A., Krivtsov, A.V., Armstrong, S.A., and Roeder, R.G. (2017). A UTX-MLL4-p300 transcriptional regulatory network coordinately shapes active enhancer landscapes for eliciting transcription. *Mol. Cell* **67**, 308–321.e6.

Lai, B., Lee, J.E., Jang, Y., Lifeng, W., Peng, W., and Ge, K. (2017). MLL3/MLL4 are required for CBP/p300 binding on enhancers and super-enhancer formation in brown adipogenesis. *Nucleic Acids Res.* **45**, 6388–6403.

Dhar, S.S., Zhao, D., Lin, T., Gu, B., Pal, K., Wu, S.J., Alam, H., Lv, J., Yun, K., Gopalakrishnan, V., Flores, E.R., Northcott, P.A., Rajaram, V., Li, W., Shilatifard, A., Sillitoe, R.V., Chen, K., and Lee, M.G. (2018). MLL4 is required to maintain broad H3K4me3 peaks and super-enhancers at tumor suppressor genes. *Mol. Cell* **70**, 825–841.e6.

Malvin, J., Zhang, X., Stumpf, P.S., Zhang, L., Peng, H., Hettige, N., Theroux, J.-F., Aouabed, Z., Wilson, K., Deshmukh, S., et al. (2022). Kabuki syndrome stem cell models reveal locus specificity of histone methyltransferase 2D (KMT2D/MLL4). *Hum. Mol. Genet.* **31**, 3715–3728.

Siebel, C., and Lendahl, U. (2017). Notch signaling in development, tissue homeostasis, and disease. *Physiol. Rev.* **97**, 1235–1294.

Gioftsidi, S., Relaix, F., and Mourikis, P. (2022). The Notch signaling network in muscle stem cells during development, homeostasis, and disease. *Skelet. Muscle* **12**, 1–12.

Sprinzak, D., and Blacklow, S.C. (2021). Biophysics of Notch signaling. *Annu. Rev. Biophys.* **50**, 157–189.

Jo, Y.W., Park, I., Yoo, K., Woo, H.Y., Kim, Y.L., Kim, Y.E., Kim, J.H., and Kong, Y.Y. (2022). Notch1 and Notch2 signaling exclusively but cooperatively maintain fetal myogenic progenitors. *Stem Cells* **40**, 1031–1042.

White, R.B., Biérinx, A.S., Gnocchi, V.F., and Zammit, P.S. (2010). Dynamics of muscle fibre growth during postnatal mouse development. *BMC Dev. Biol.* **10**, 21.

Mukund, K., and Subramaniam, S. (2020). Skeletal muscle: A review of molecular structure and function, in health and disease. *Wiley Interdiscip. Rev. Syst. Biol. Med.* **12**, e1462.

Yin, H., Price, F., and Rudnicki, M.A. (2013). Satellite cells and the muscle stem cell niche. *Physiol. Rev.* **93**, 23–67.

Relaix, F., Bencze, M.J., Borok, M.J., Der Vartanian, A., Gattazzo, F., Mademtzoglou, D., Perez-Diaz, S., Prola, A., Reyes-Fernandez, P.C., Rotini, A., and Taglietti, A. (2021). Perspectives on skeletal muscle stem cells. *Nat. Commun.* **12**, 1–11.

Eliazer, S., Muncie, J.M., Christensen, J., Sun, X., D'Urso, R.S., Weaver, V.M., and Brack, A.S. (2019). Wnt4 from the niche controls the mechano-properties and quiescent state of muscle stem cells. *Cell Stem Cell* **25**, 654–665.e4.

Zhao, P., and Hoffman, E.P. (2004). Embryonic myogenesis pathways in muscle regeneration. *Dev. Dyn.* **229**, 380–392.

Zofkie, W., Southard, S.M., Braun, T., and Lepper, C. (2021). Fibroblast growth factor 6 regulates sizing of the muscle stem cell pool. *Stem Cell Rep.* **16**, 2913–2927.

Goel, A.J., Rieder, M.K., Arnold, H.H., Radice, G.L., and Krauss, R.S. (2017). Niche cadherins control the quiescence-to-activation transition in muscle stem cells. *Cell Rep.* **21**, 2236–2250.

Schuster-Gossler, K., Cordes, R., and Gossler, A. (2007). Premature myogenic differentiation and depletion of progenitor cells cause severe muscle hypotrophy in Delta1 mutants. *Proc. Natl. Acad. Sci. USA* **104**, 537–542.

Yartseva, V., Goldstein, L.D., Rodman, J., Kates, L., Chen, M.Z., Chen, Y.J.J., Foreman, O., Siebel, C.W., Modrusan, Z., Peterson, A.S., and Jovičić, A. (2020). Heterogeneity of satellite cells implicates DELTA1/NOTCH2 signaling in self-renewal. *Cell Rep.* **30**, 1491–1503.e6.

Zhang, Y., Lahmann, I., Baum, K., Shimojo, H., Mourikis, P., Wolf, J., Kageyama, R., and Birchmeier, C. (2021). Oscillations of Delta-like1 regulate the balance

between differentiation and maintenance of muscle stem cells. *Nat. Commun.* **12**, 1–14.

Low, S.H., Barnes, J.L., Zammit, P.S., and Beauchamp, J.R. (2018). Delta-Like 4 activates Notch 3 to regulate self-renewal in skeletal muscle stem cells. *Stem Cells* **36**, 458–466.

Liu, L., Ding, C., Fu, T., Feng, Z., Lee, J.E., Xiao, L., Xu, Z., Yin, Y., Guo, Q., Sun, Z., et al. (2020). Histone methyltransferase MLL4 controls myofiber identity and muscle performance through MEF2 interaction. *J. Clin. Invest.* **130**, 4710–4725.

Pette, D., and Staron, R.S. (2000). Myosin isoforms, muscle fiber types, and transitions. *Microsc. Res. Tech.* **50**, 500–509.

Brü, J.C., Dodson, M., Winnay, J.N., Hayashi, T., Hö, D., Accili, D., Goodyear, L.J., and Kahn, R. (1998). A muscle-specific insulin receptor knockout exhibits features of the metabolic syndrome of NIDDM without altering glucose tolerance. *Mol. Cell* **2**, 101–106.

Cramer, A.A., Prasad, V., Eftestøl, E., Song, T., Hansson, K.A., Dugdale, H.F., Sadayappan, S., Ochala, J., Gundersen, K., and Millay, D.P. (2020). Nuclear numbers in syncytial muscle fibers promote size but limit the development of larger myonuclear domains. *Nat. Commun.* **11**, 1–12.

Augusto, V., Padovani, C.R., and Rocha Campos, G.E. (2004). Skeletal muscle fiber types in C57Bl6J mice. *Braz. J. Morphol. Sci.* **21**, 1–9.

Seo, J.Y., Kang, J.S., Kim, Y.L., Jo, Y.W., Kim, J.H., Hann, S.H., Park, J., Park, I., Park, H., Yoo, K., et al. (2021). Maintenance of type 2 glycolytic myofibers with age by Mib1-Actn3 axis. *Nat. Commun.* **12**, 1–11.

Bjornson, C.R.R., Cheung, T.H., Liu, L., Tripathi, P.V., Steeper, K.M., and Rando, T.A. (2012). Notch signaling is necessary to maintain quiescence in adult muscle stem cells. *Stem Cells* **30**, 232–242.

Musarò, A. (2014). The basis of muscle regeneration. *Adv. Biol.* **2014**, 1–16.

Skelly, D.A., Squiers, G.T., McLellan, M.A., Bolisetty, M.T., Robson, P., Rosenthal, N.A., and Pinto, A.R. (2018). Single-cell transcriptional profiling reveals cellular diversity and intercommunication in the mouse heart. *Cell Rep.* **22**, 600–610.

Mourikis, P., Sambasivan, R., Castel, D., Rocheteau, P., Bizzarro, V., and Tajbakhsh, S. (2012). A critical requirement for Notch signaling in maintenance of the quiescent skeletal muscle stem cell state. *Stem Cells* **30**, 243–252.

Kann, A.P., and Krauss, R.S. (2019). Multiplexed RNAscope and immunofluorescence on whole-mount skeletal myofibers and their associated stem cells. *Development* **146**, dev178970.

Haizlip, K.M., Harrison, B.C., and Leinwand, L.A. (2015). Sex-based differences in skeletal muscle kinetics and fiber-type composition. *Physiology* **30**, 30–39.

Takahashi, F., Baba, T., Christianto, A., Yanai, S., Lee-Okada, H.C., Ishiwata, K., Nakabayashi, K., Hata, K., Ishii, T., Hasegawa, T., Yokomizo, T., Choi, M.H., and

Morohashi, K. (2024). Development of sexual dimorphism of skeletal muscles through the adrenal cortex, caused by androgen-induced global gene suppression. *Cell Rep.* **43**, 102482.

Kitamura, T., Kitamura, Y.I., Funahashi, Y., Shawber, C.J., Castrillon, D.H., Kollipara, R., DePinho, R.A., Kitajewski, J., and Accili, D. (2007). A Foxo/Notch pathway controls myogenic differentiation and fiber type specification. *J. Clin. Invest.* **117**, 2477–2485.

Zhou, J., So, K.K., Li, Y., Yuan, J., Ding, Y., Chen, F., Huang, Y., Liu, J., Lee, W., Li, G., Ju, Z., Sun, H., and Wang, H. (2019). Elevated H3K27ac in aged skeletal muscle leads to increase in extracellular matrix and fibrogenic conversion of muscle satellite cells. *Aging Cell* **18**, e13003.

Lazure, F., Blackburn, D.M., Corchado, A.H., Sahinyan, K., Karam, N., Sharanek, A., Nguyen, D., Lepper, C., Najafabadi, H.S., Perkins, T.J., Jahani-Asl, A., and Soleimani, V.D. (2020). Myf6/MRF4 is a myogenic niche regulator required for the maintenance of the muscle stem cell pool. *EMBO Rep.* **21**, e48961.

Rao, R.C., and Dou, Y. (2015). Hijacked in cancer: The KMT2 (MLL) family of methyltransferases. *Nat. Rev. Cancer* **15**, 334–346.

Ang, S.Y., Uebersohn, A., Spencer, C.I., Huang, Y., Lee, J.E., Ge, K., and Bruneau, B.G. (2016). KMT2D regulates specific programs in heart development via histone H3 lysine 4 di-methylation. *Development* **143**, 810–821.

Fujimaki, S., Seko, D., Kitajima, Y., Yoshioka, K., Tsuchiya, Y., Masuda, S., and Ono, Y. (2018). Notch1 and Notch2 coordinately regulate stem cell function in the quiescent and activated states of muscle satellite cells. *Stem Cells* **36**, 278–285.

Fukada, S.I., Yamaguchi, M., Kokubo, H., Ogawa, R., Uezumi, A., Yoneda, T., Matev, M.M., Motohashi, N., Ito, T., Zolkiewska, A., Johnson, R.L., Saga, Y., Miyagoe-Suzuki, Y., Tsujikawa, K., Takeda, S., and Yamamoto, H. (2011). Hesr1 and Hesr3 are essential to generate undifferentiated quiescent satellite cells and to maintain satellite cell numbers. *Development* **138**, 4609–4619.

Noguchi, Y.T., Nakamura, M., Hino, N., Nogami, J., Tsuji, S., Sato, T., Zhang, L., Tsujikawa, K., Tanaka, T., Izawa, K., Okada, Y., Doi, T., Kokubo, H., Harada, A., Uezumi, A., Gessler, M., Ohkawa, Y., and Fukada, S.I. (2019). Cell-autonomous and redundant roles of Hey1 and HeyL in muscle stem cells: HeyL requires Hes1 to bind diverse DNA sites. Development 146, dev174441.

Huisman, C., Kim, Y.A., Jeon, S., Shin, B., Choi, J., Lim, S.J., Youn, S.M., Park, Y., Medha, K.C., Kim, S., Lee, S.K., Lee, S., and Lee, J.W. (2021). The histone H3-lysine 4-methyltransferase Mll4 regulates the development of growth hormone-releasing hormone-producing neurons in the mouse hypothalamus. Nat. Commun. 12, 4899.

Esteves de Lima, J., Bonnin, M.A., Birchmeier, C., and Duprez, D. (2016). Muscle contraction is required to maintain the pool of muscle progenitors via YAP and NOTCH during fetal myogenesis. eLife 5, e15593.

Bi, P., Yue, F., Sato, Y., Wirbisky, S., Liu, W., Shan, T., Wen, Y., Zhou, D., Freeman, J., and Kuang, S. (2016). Stage-specific effects of Notch activation during skeletal

myogenesis. eLife 5, e17355.

Gallot, Y., Hindi, S., Mann, A., and Kumar, A. (2016). Isolation, culture, and staining of single myofibers. Bio-protocol 6, e1963.

Liu, L., Cheung, T.H., Charville, G.W., and Rando, T.A. (2015). Isolation of skeletal muscle stem cells by fluorescence-activated cell sorting. Nat. Protoc. 10, 1612–1624.

국문 초록

근육줄기세포군 유지를 위한
근섬유 내 Mll4의 역할 연구

근육 줄기세포는 골격근에 상주하는 줄기 세포로, 근육의 발생과 성장 및 재생에 중요한 역할을 한다. 근육 성장이 활발히 일어나는 사춘기 시기까지 근육 줄기세포는 꾸준히 증식하고 근세포로 분화하면서 세포 융합을 통해 근섬유를 형성한다. 성체에서 근육 줄기세포는 정지상태(quiescence)에 돌입해 예비 줄기세포군으로 유지된다. 근육에 부상 등의 스트레스가 가해지면 예비 줄기세포군이 활성화되어 근육 조직을 복구하기 위한 근세포로 분화한다. 이처럼 근육줄기세포는 일생의 전반에 걸쳐 근육의 발달 및 재생을 위해 정지, 활성화, 증식 및 분화를 반복한다. 따라서 근육의 정상적인 기능을 유지하기 위해 근육 줄기세포의 군집을 유지하는 것이 중요하다.

본 연구에서는 근섬유에서 발현하는 Mll4 단백질이 성장기와 성체기의 근육 줄기세포 군집 형성 및 유지에 중요한 역할을 함을 밝혔다. 근섬유 특이적으로 Mll4 유전자를 제거한 마우스의 근육을 사춘기 시기에 관찰한 결과, 정지상태로 돌입해야 하는 근육 줄기세포들이 여전히 활성 상태를 유지하며 지속적으로 분화하는 양상을 띄었다. 이것은 궁극

적으로 성체 근육에서의 근육 줄기세포군 감소로 이어졌다. 성체 시기 근섬유에서 Mll4 유전자를 제거하면 정지상태로 유지되어야 하는 근육 줄기세포가 비정상적으로 활성화되며 증식과 분화를 거듭해 근육 줄기세포군의 고갈로 이어졌다. 근섬유 Mll4의 제거에 의한 근육 줄기세포 고갈 현상은 근섬유 내 Notch 리간드의 발현 감소와 동반되었다. 사춘기 시기 근섬유에서는 Jag1과 Dll1, 성체 근섬유에서는 Jag2와 Dll4가 감소하면서 근육 줄기세포 내 Notch 신호가 감소했고 이에 따른 정지상태 돌입 혹은 유지에 실패했다.

본 연구 결과는 근섬유에서 발현하는 Mll4가 Notch 신호를 통해 사춘기 시기에 근육 줄기세포군 형성과 성체의 근육 줄기세포군 유지에 중요한 조절자라는 결론을 제시한다. 선행 연구들과 더불어 근육 줄기세포군을 유지하는 메커니즘을 추가적으로 밝힘으로써 근육 줄기세포의 생물학적 조작 가능성을 확대하고 근육의 건강 증진을 위한 연구에 기여할 수 있다.

주요어: 골격근, 근육 줄기세포, 근육 형성, 근육 손상, Mll4, Notch 신호

학번: 2020-25562